EXAMINATION OF A METHOD: TESTING THE KELLEY-BARTON METHOD ON THE HERÐUBREIÐ TUYA, NORTHERN VOLCANIC ZONE, ICELAND

Undergraduate Research Thesis
Submitted in partial fulfillment of the requirements for graduation
with research Distinction in Earth Sciences in the undergraduate colleges
of The Ohio State University

By

Collin A. Oborn
The Ohio State University
2018

Approved by

Michael Barton

Michael Barton, Project Advisor
School of Earth Sciences

TABLE OF CONTENTS

ABSTRACT

Iceland is the most volcanically diverse location on the planet as nearly every type of volcano can be found on this island. Volcanoes are an existential and powerful threat to the modern world on both short and long time scales, and understanding their inner workings is a necessary first step in protecting society from one of nature's deadliest and most destructive activities. This study focused on a specific locality in Iceland's Northern Volcanic Zone, the volcano known as Herdubreid (Herðubreið). The purpose of this research was to determine the depth of crustal magma bodies that feed Herdubreid using a new method developed by Dr. Michael Barton and Dr. Daniel Kelley. Their method involved using the analyzed weight percent of major oxides in recently collected samples of glass to calculate the pressure at which the magmas partially crystalized. From this pressure, the relative depth of the magma chamber or chambers located in the underlying crust can be established. The interpretation of these depths revealed the presence of two main magma bodies located at 9–11 km, and 15–18 km below the surface. These depths agree with the results of seismic and geodetic studies for the surrounding areas and are consistent with results obtained using identical petrologic methods to the one used in this study for Herdubreid and other volcanic plumbing systems in Iceland. This work provides only part of the bigger picture of Icelandic volcanism, as Herdubreid is only one of about thirty active volcanoes on Iceland. While the results of this work constitute a necessary first step for improving warning systems and updating evacuation procedures for people who live or work near similar types of volcanoes, more work is needed to gain a complete picture of the magma plumbing systems in the crust beneath Iceland. Additional research is underway to collect and study samples from these volcanic systems with the objective of understanding how these different types of volcanoes work, how the different plumbing systems interact with each other, and how to place the results obtained for Iceland into a global context.

ACKNOWLEDGEMENTS

I want to extend my deepest gratitude to Dr. Michael Barton and his former graduate assistants Dr. Jamison Scott and Dr. Dan Kelley and his current research group for all of their guidance and support for my work on this project. I would especially like to thank Dr. Kelley and his research assistant Jenna Reindel, for collecting and analyzing samples. Without their data this project would not have been possible. I would also like to thank Dr. Anne Carey for her guidance and advice in writing this thesis and applying to graduate programs, Dr. Joachim Moortgat for challenging me and for showing me that I have the confidence to succeed in unfamiliar environments and for his advice on graduate school applications, and Dr. Christena Cox and Angeletha Rogers for giving me the opportunity to work as a teaching assistant and enhance my teaching skills. A huge thank you goes out to Shell Exploration and Production Company, Friends of Orton Hall, and the Ohio State Office of Undergraduate Research and Creative Inquiry for providing funding for this research and allowing me the opportunity to perform research in the field. I am also grateful for the scholarships provided by The Ohio State University, the Ohio State University Marching Band Alumni Association, and the Katz Endowment.

Outside of the School of Earth Sciences, I want to thank Professor John Murray and Lecturer Tiernan Henry of NUI Galway and Eamon Doyle of the Burren and Cliffs of Moher Geopark for making my field camp experience one to remember. I would also like to thank my parents for their love and support no matter my decisions and despite my winding career path through college. You taught me to be independent and I will appreciate your trust in my decision making for years to come.

From my years of marching band, thank you Buddy, Rusty, Fozz, Meaty, Lightning, AK, Helga, Derp, Snorlax, Olaf, Sticky, Van Gogh, Chicken Farmer, Blackhawk, Darla, Badger, DB, Tebow, Pretzel, Sunny D, The Tranimal, Vijay, Trevor, and Jeff. You all have been instrumental in my growth into the person I am today. I love all of you and I will miss you. Thank you to all of the wonderful friends I have met in my earth Science classes: Matt, Aaron, Casey, Chandler, Luke, and Seth. The last three years would not have been the same without you. Lastly, I would like to thank Ally Brady, assisting in my fieldwork and for constantly supporting me through my final year at Ohio State.

LIST OF FIGURES

LIST OF TABLES

INTRODUCTION

Dr. Daniel Kelley and Dr. Michael Barton have developed a method for calculating the pressure of partial crystallization for glassy basalts that represent the liquids from which they crystallized (Kelley and Barton, 2008). Iceland is the ideal location for testing the limits of this method. Lying at the intersection of the Mid Atlantic Ridge and a mantle plume, Iceland is incredibly volcanically diverse, with over 30 volcanic systems present on the island covering every known volcano type with the exception of diatremes (Sturkell et al., 2006; Thordarson and Larsen, 2007). Knowing the depths of magma chambers are of interest for four main reasons, as outlined in Kelley and Barton (2008). The first reason these depths are of interest is that they are important in predicting and forecasting eruption as they provide insights on interpreting precursory activities (deformation, gas emissions, earthquake swarms, etc.). Second, melt compositions and phase relationships vary with pressure (Yang et al., 1996) and therefore magma chamber depths can help constrain magma evolution models. Third, magma body distribution is key to understanding thermal gradients that affect crustal density and seismic velocity variations. Lastly, knowledge of the size and location of magma chambers is necessary to understanding the mechanisms of crustal accretion and differentiation.

Recently, geodetic methods have been at the forefront of estimating magma chamber depths (Sturkell et al., 2006). Studies utilizing geodetic techniques have produce results that often agree with those obtained via geophysical methods. Using GPS and the satellite-based InSAR, these geodetic studies have been able to measure ground movement over large areas and at specific localities with and ever increasing resolution (Tilling et al., 1987). While geophysical, geodetic, and petrological methods like the one described by Kelley and Barton (2008) can provide information on active volcanic systems, the Kelley-Barton method can also provide insights on inactive volcanic systems. Petrological examinations like the Kelley-Barton method can provide information on magmatic processes occurring within the reservoirs and their distribution.

When direct comparison is available, depth estimates from petrological methods agree well with other geophysical and geodetic studies. However, many of the petrological results reported for Icelandic magmas are only qualitative. This research takes a quantitative approach in which the pressure and temperature are calculated from liquid compositions in equilibrium with olivine, plagioclase, and clinopyroxene using Kelley-Barton method (2008). In this method pressures are calculated with an accuracy of ±126 MPa and depths are calculated from the pressures assuming a constant crustal density of that of basalt (2900 kg/m^3).

Depths of the magma chambers were calculated for the volcano Herdubreid using data compiled from Moore and Calk (1991) and an unpublished dataset collected and analyzed by Dr. Daniel Kelley and one of his students, Jenna Reindel. Though it is not used in this study, the collection location for the samples in the former dataset are provided in Moore and Calk (1991) and the map of these locations is taken from the same study and shown in *Figure 1*. The potential relevance of this information is discussed in the Recommendations for Future Work section near the end of this thesis. The magma chamber depth estimates obtained in this study appear to be accurate when compared to various geophysical and geodetic studies of Herdubreid and the surrounding areas. The implications for magma evolution as it relates to the distribution of magma chambers and chemical compositions is also discussed.

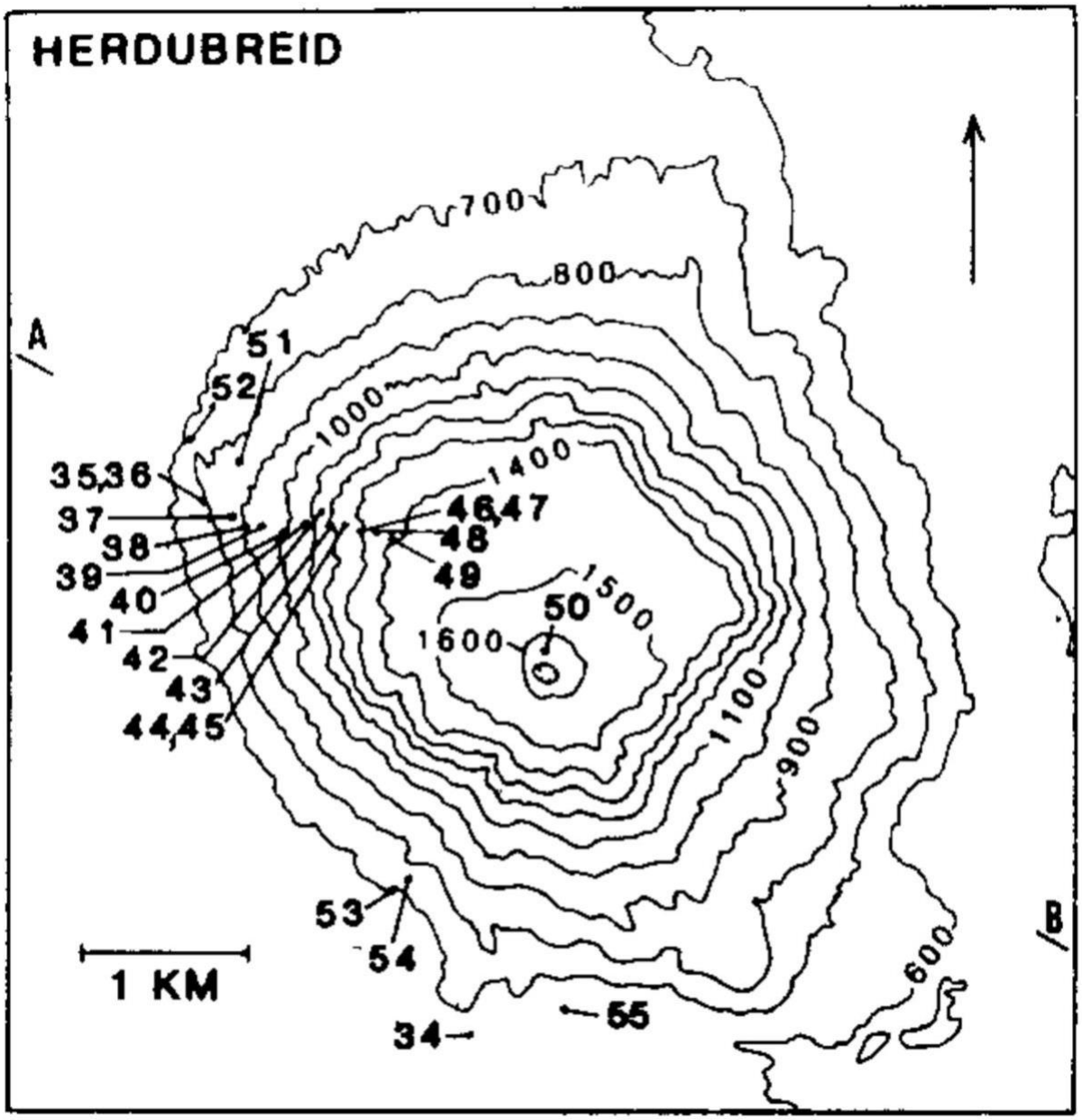

Figure 1: Map of sample locations around Herdubreid. From Moore and Calk (1991).

GEOLOGIC SETTING

At ~103,000 km^2, Iceland is a small basaltic island, 10–40 km thick, that sits on a ~350,000 km^2 plateau that rises more than 3000 m above the surrounding sea floor (Gudmundsson, 2000). It is thought that it formed from volcanic activity brought about by Iceland's position over two major submarine land forms (Thordarson and Larsen, 2007), the Greenland—Iceland—Faeroe Ridge and the Mid-Atlantic Ridge (*Figure 2*). The formation of this plateau, thought to have begun ~24 million years ago (Óskarsson et al., 1985), and is considered to be the result of the interaction of the Mid-Atlantic spreading zone and a mantle plume (Vink, 1984). Iceland's mantle plume has been active for the last 65 million years, forming the North Atlantic Igneous Province (NAIP). Iceland is only remaining active area of this roughly 2000 km long province (Saunders et al., 1997).

Neovolcanic zones *(Figure 3)* are 15–50 km wide belts of volcanism and active faulting that serve as surficial representations of Iceland's past volcanic history. The axial volcanic zone is the largest neovolcanic zone in Iceland. Lying on the plate boundary and connecting the Reykjanes and Kolbeinsey Ridge, the axial volcanic zone is composed of the Western Volcanic Zone (WVZ) connected to the Northern Volcanic Zone (NVZ) by the Mid Iceland Belt (MIB). In the south, at the town of Reykjanes, the WVZ connects to the Reykjanes Ridge via a subset of volcanic systems that is sometimes referred to as the Reykjanes Volcanic Zone (RVZ) (Thordarson and Larsen, 2007). In the north, the NVZ connects to the Kolbeinsey Ridge near Öxarfjördur via an area of active faulting known as the Tjörnes Fracture Zone (TFZ). The Eastern Volcanic Zone (EVZ) is the result of a currently southward propagating axial rift that will eventually replace the WVZ as the connecting zone to the Reykjanes Ridge. The main difference between these two axial zones is erupted magma compositions as the main axial volcanic zone is characterized by entirely tholeiitic magmatism while the EVZ sees a change from tholeiitic magmas in the northeastern segment to mildy alkalic magmas in the southwest segment of the EVZ (Jakobsson, 1979). There are two minor zones of volcanism in Iceland that are characterized by alkali magmatism. In *Figure 3* these are labeled as the Eastern Flank Zone (EFZ) and the Western Flank Zone (WFZ), also known as the Öræfi Volcanic Belt and the Snæfellsnes Volcanic Belt respectively. These intraplate volcanic belts are in vastly different stages of their lives, as the WFZ is an old rift zone, reactivated ~2 Ma, propagating east-southeast (Gudmundsson, 2000) while the EFZ may represent a newly developing rift (Thordarson and Höskuldsson, 2002).

A classification for Icelandic volcanoes that compose these neovolcanic zones was proposed by Thórarinsson (1981) that is based on the nature of vent products and vent forms. The first parameter for this classification is the vent system geometry, wherein vents are classified as a point or linear source. The point source category includes circular vent systems and vent systems that began as short fissures but were quickly reduced to one vent. The linear source classification simply represents vent systems demarked as fissures. The second parameter used in this classification scheme is the type of deposits characterizing the erupted products (i.e. ash, clastogenic lava, lava, scoria, or spatter). This classification is useful for the classification of monogenetic basalt volcanoes that typify Icelandic fissure swarms and is presented in *Table 1*.

In the Thórarinsson (1981) classification, Herdubreid is defined as a subglacial/submarine, circular vent erupting effusive, then explosive, then effusive products over the course of its formation, and is also known as a Table Mountain. This type of volcano is widely present in Iceland due, in part, to high glaciation during recent eruptive history and is represented by both

central vent and linear vent systems that currently exhibit distinctive landforms in the non-glaciated parts of the neovolcanic zones and beneath present glaciers (Gudmundsson et al., 2002). If there is sufficient ice pressure over an erupting basaltic lava, then pillow lavas are formed (Hoskuldsson and Sparks, 1997). If eruption stops at this initial stage then pillow lava cones or ridges are formed. In continued eruption, the activity changes from effusive products to explosive phreatomagmatic products that form móberg cones or ridges if eruption ends in this stage. The final stage occurs when eruption continues until the volcanic ediface emerges from the surface of the ice, causing effusive activity to resume. Eruptions that reach this stage produce tuyas or table mountains composed of lava deltas and subaerial flows. These three stages of eruption are shown in *Figure 4*.

However, there is evidence that the formation of Herdubreid was more complicated than the simple explanation above. Herdubreid may not be a stand-alone system, due to the presence of Herdubreidartögl, a nearby ridge that can be linked to the eruption events that formed Herdubreid (Werner et al., 1996). In Werner at al. (1996), the model proposed for the eruptions that formed Herdebreid includes four stages that can be linked to four stratigraphic units (*Figure 5)* via rock structures, textures, and deposit compositions and hyaloclastite alteration degrees and matrix glass volatile contents. When combined, these aspects indicate the evolution for the four units within specific environments that reflect climate changes over the last 100,000 years in Iceland (Jakobsson, 1978; Sigvaldason et al., 1992; Tómasson, 1993). The history of these four eruption periods is as follows:

1. Primitive olivine tholeiites erupted in the southern area of Herdubreidartögl, building a subaerial shield volcano. Volcanic activity may have stopped at the beginning of the last glaciation due to ice accumulation causing excess lithostatic pressure on the magma reservoir.
2. Once glaciation had reached a maximum and the overlying ice sheet began to thin, the eruption center began the second stage of growth in a waning lacustrine environment. Olivine tholeiites were first deposited, followed by subaqueously produced hyaloclastites that were redeposited by mass flows. As Herdubreid grew towards the lake's surface, it began producing effusive and hydroclastic deposits until it finally emerged above the surface, producing subaerial lava flows once again (*Figure 6*).
3. The last glacial maxima 12–15 kya caused the thickening of the ice sheet over Herdubreid, where it then produces pillow lavas under steep-sided hyaloclastite deposits in the classic Table Mountain subglacial environment. Once the volcano melted through the glacier it covered the exposed pillows and hyaloclastites in subaerial flows and agglutinates (*Figure 6*). During this time, both Herdubreid and Herdubreidartögl produced the most evolved tholeiites of any eruption period within this model.
4. By the time glaciation subsided, volcanic activity had ceased at Herdubreid, but subaerial eruptions at Herdubreidartögl continued to produce fallout deposits and olivine tholeiitic lava flows.

Since the events outlined in the Werner et al. (1996), Herdubreid has been volcanically inactive. It is not clear whether it lies within the fissure swarms of the nearby Askja or Kverkfjöll active volcanic systems (*Figure 7*) but Herdubreid is not considered active (Thordarson and Larsen, 2007).

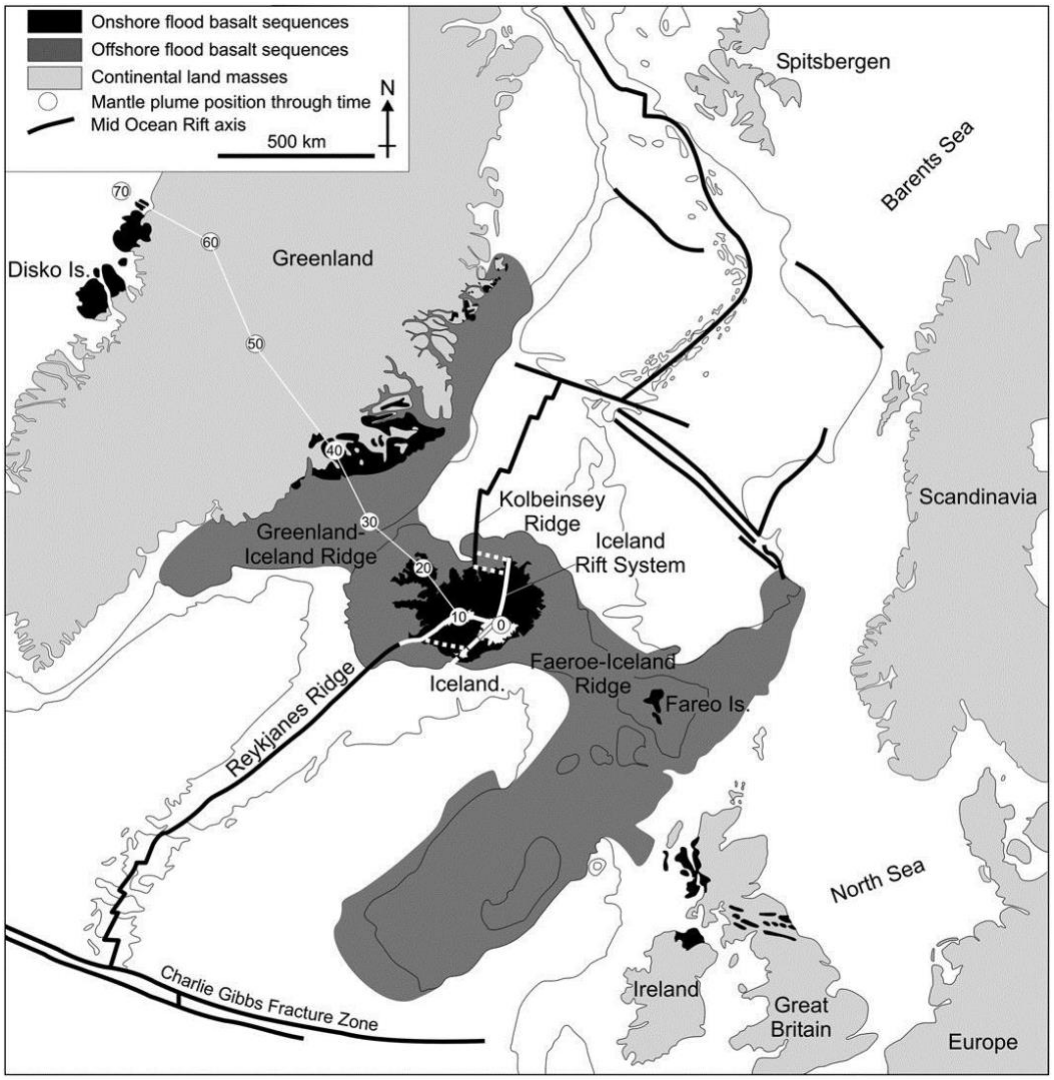

Figure 2: Map of the North Atlantic showing the structural context for Iceland. The elevated plateau that Iceland sits on is situated at the junction of the Kolbeinsey and Reykjanes Ridge segments. The axis of the submarine sections of the Mid-Atlantic ridge are represented by a thick black line and above sea-level segment in Iceland is represented by a thick white line. Dashed lines indicate fault zones and the line with numbered circles shows the position of the Iceland mantle plume over the last 70 million years. From (Thordarson and Larsen, 2007).

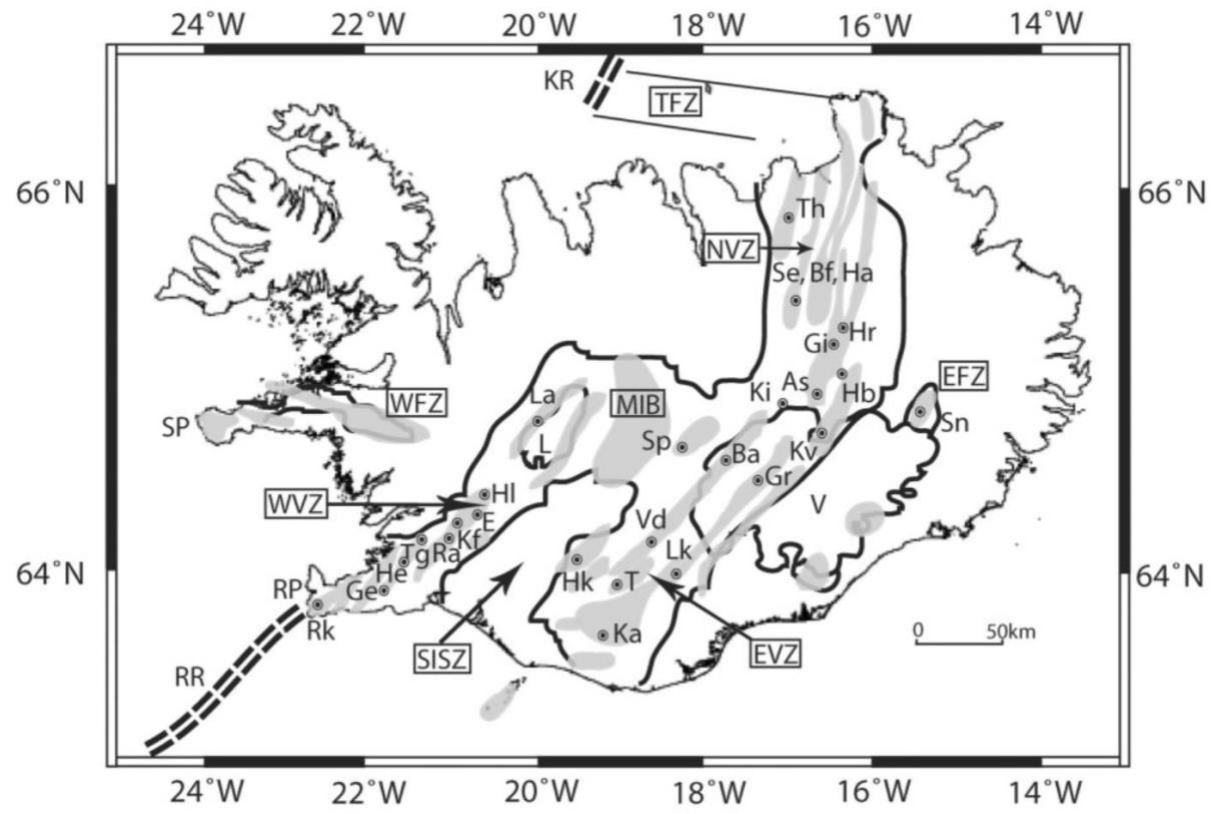

Figure 3: Map of Iceland showing the locations of important geological features. Herdubreid, Askja, and Kverkfjöll are labeled as Hb, As, and Kv respectively. Major zones of volcanism, minor flank zones, and faulting are labeled: WVZ, Western Volcanic Zone; EVZ, Eastern Volcanic Zone; NVZ, Northern Volcanic Zone; WFZ, Western Flank Zone; EFZ, Eastern Flank Zone; MIB, Mid Icelandic Belt; SISZ, South Iceland Seismic Zone; TFZ, Tjörnes Fracture Zone. Other principal geologic elements are labeled: RR, Reykjanes Ridge; KR, Kolbeinsey Ridge; RP, Reykjanes Peninsula; SP, Snæfellsnes Peninsula; L, Langjökull Glacier; V, Vatnajökull Glacier. From Kelley and Barton (2008).

Table 1: Classification of Icelandic volcanoes proposed by Sigurdur Thórarinsson and modified by Thorarson and Larsen (2007). Rows are separated by eruption environment (subaerial magmatic, subaerial phreatomagmatic, and subglacial/submarine) and eruption type (Effusive, Explosive, Effusive–explosive/less explosive, and Effusive–explosive–effusive) while columns are separated by vent form (circular or linear). Horizontal lines have been added to better distinguish the rows from one another.

Classification of basaltic volcanoes in Iceland

Eruption characteristics		Circular (central vent or short fissure)	Examples	Linear (long fissure)	Examples
Environment	Eruption type				
Subaerial magmatic	Effusive–less explosive (flood lava)	Lava shield	Skjaldbreidur, Kollóttadyngja	Mixed cone row	Laki, Eldgjá
	Effusive	Spatter ring (eldborg)	Eldborg at Mýrar, Búrfell in Heidmörk	Spatter cone row	Tröllagígar, Threngslaborgir
	Effusive–explosive	Scoria cone	Eldfell, Grábrók	Scoria cone row	Vikraborgir,
	Explosive			Volcanigenic chasms	Valagjá
Subaerial phreatomagmatic	Explosive	Tephra (tuff) cone, tephra (tuff) ring	Hrossaborg, Hverfjall ?	Tephra (tuff) cone row, tephra (tuff) ring row	Vatnaöldur, Veidivötn[a]
		Maar	Grænavatn, Víti	Maar crater row	?
Subglacial and submarine	Effusive	Pillow lava cone	?	Pillow lava ridge	Kverkfjallarani
	Effusive–explosive	Móberg cone seamount	Keilir Jólnir	Móberg ridge or submarine ridge	Sveifluhals, Eldeyjarbodi
	Effusive–explosive–effusive	Table mountain	Herdubreid	Table mountain (ridge-like)	Bláfjall

Modified from Thorarinsson (1981). ?: no examples are known.
[a] Svartikrókur segment.

Figure 4: Stages of growth for a Table Mountain formed from a subglacial eruption, taken from (Jones, 1968): (a) pillow lava cone/ridge, (b)móberg cone or ridge forms, and (c)table mountain as described in, and borrowed from, Thordarson and Larsen (2007).

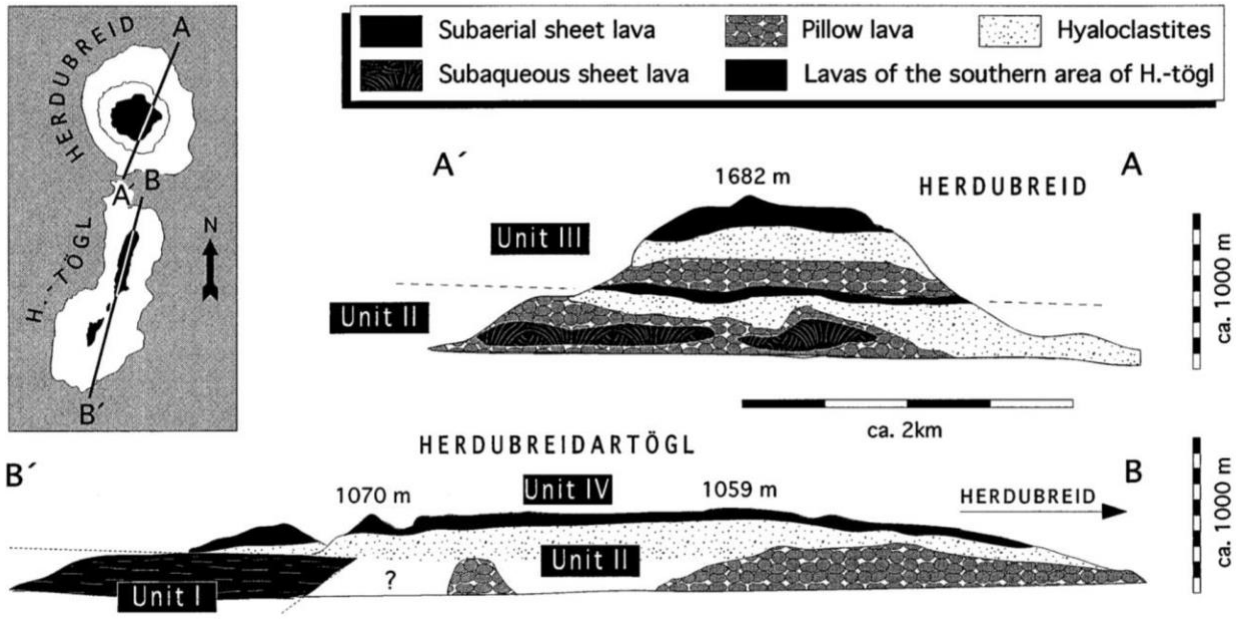

Figure 5: Major units displayed in simple cross sections of Herdubreid and Herdubreidartögl. The double layered table mountain succession can be seen in this view, developing from pillow lavas to hyaloclastites to subaerial lavas in both Unit II and Unit III. The two units show a distinct mineralogical difference and are therefore separated by dashed line. From Werner et al. (1996).

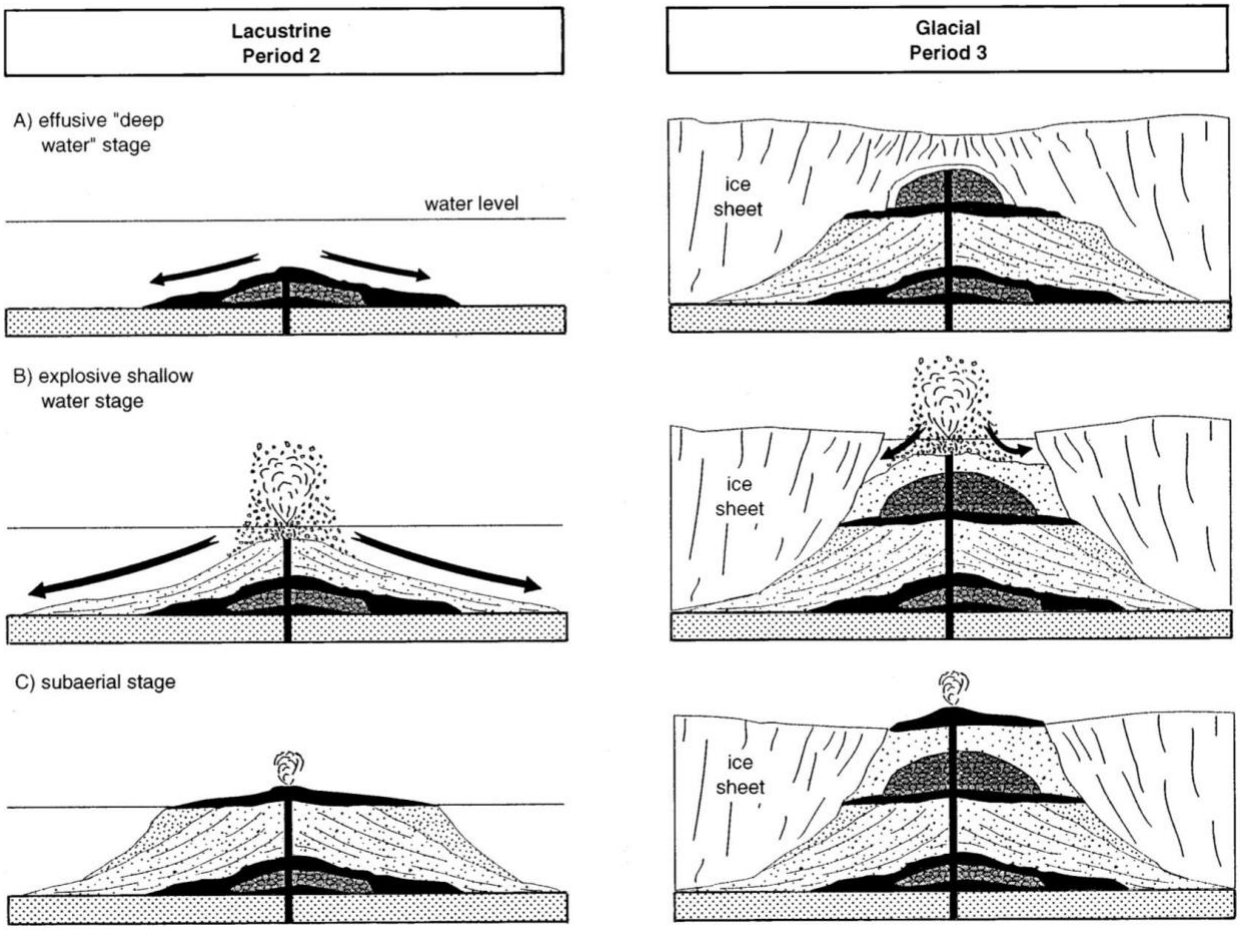

Figure 6: Simplified sketches of the second and third growth periods for the Herdubreid volcano displaying the difference between table mountain formation in subglacial and lacustrine environments. From Werner et al. (1996).

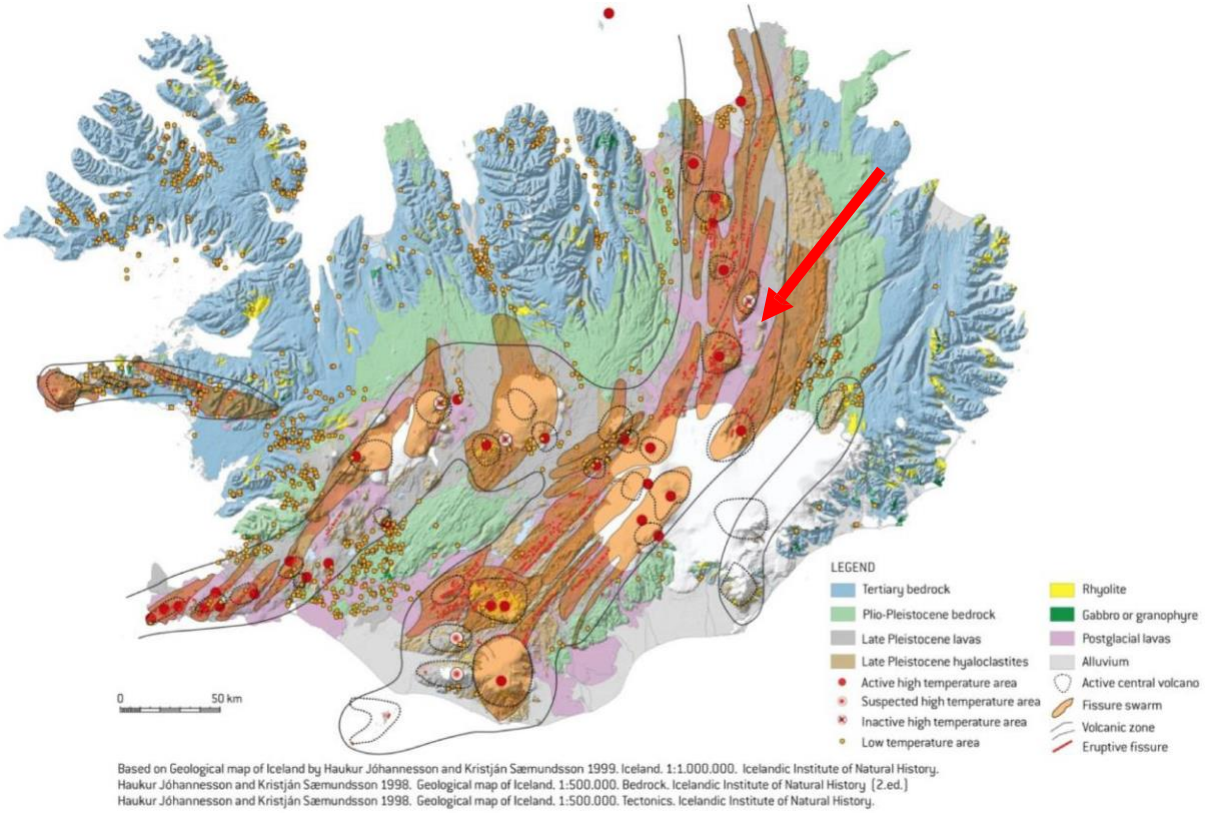

Figure 7: Geologic map of Iceland created with (Jóhannesson and Saemundsson, 1998; Jóhannesson and Sæmundsson, 1998; Jóhannesson and Sæmundsson, 1999) by (Mortensen, 2013). Mortensen depicts the volcanic systems of Iceland. A red arrow shows that Herdubreid lies between two systems, but not within either.

METHODS

Pressures of Crystallization

Magma chamber depth beneath Herdubreid can be estimated using the pressure at which crystallization occurs before magma is erupted, referred to as pressure of partial crystallization. Because pressure (P) is positively correlated with depth (z), depth can be estimated from the pressure of partial crystallization, which can be calculated using an array of petrological techniques. For this study, I used a quantitative petrologic method described by Kelley and Barton (2008) that calculates pressures based on the chemical compositions and analyses of glasses. The analyses in datasets used in this study were done by averaging multiple spot analyses of each sample obtained using an electron microprobe or scanning electron microscope (SEM). Spot analyses in the Moore and Calk (1991) dataset were already averaged. In the Kelley dataset, groups of five analyses were average with the exception of three samples, where it was determined that one of the five spot analyses had been done on olivine or plagioclase feldspar and therefore it was not included in the calculation of the average.

In order to process samples efficiently, the most appropriate method for calculating the pressures of partial crystallization relies on the comparison of natural basalt sample compositions with the compositions of liquids that lie on the pressure-dependent cotectic boundary of olivine *(ol)* plagioclase *(plag)*, and clinopyroxene *(cpx)*. Many basalts crystallize these three minerals so this method, that is based on the experimentally proven observation that the position of the *ol—plag—cpx* cotectic varies with pressure (Yang et al., 1996) is appropriate. With 10 chemical components (*Appendix I*) that dominate a basalt measured during the chemical analyses it is necessary to simplify the resulting ten-dimensional system in order to visualize the relationships among the major components. This simplification is done by reducing the 10 components down to four, defined as the Calcium, Magnesium, Aluminum, and Silicon Oxides *(CaO—MgO—Al_2O_3—SiO_2)*. Compositions can be plotted in the tetrahedron that defines a basalt once they are converted into normative mineral constituents and graphically represented by four normative minerals (*Figure 8a*). To determine the phase relationships among the four major minerals and the liquids, compositions are then projected from one of the mineral components onto ternary planes that act as pseudoternary phase diagrams. With the recalculation procedure outlined in Walker et al. (1979), phase relationships have been projected onto the *ol—cpx—qtz* pseudoternary plane from *plag* for the purpose of illustrating the effect of pressure on liquid composition (*Figure 8b*). Figure 8 shows the shift in the positions of the *ol—plag—cpx* cotectic towards olivine within increasing pressure (P). Phase relationships projected from *ol* onto the *plag—cpx—qtz* pseudoternary plane display a shift of the *ol—plag—cpx* cotectic towards *plag* with increasing P. The result of these two shifts is an overall shift in the cotectic away from *cpx*, indicating that earlier crystallization of *cpx* is favored at higher pressures and that a decrease in *CaO* with decreasing *MgO* is apparent in liquids at an earlier stage of crystallization.

Yang et al. (1996) provides three equations that describe systematic compositional changes with pressure in melts. The equations are defined as function of pressure and temperature (T), and the composition of liquids lying on the *ol—plag—cpx* cotectic. These equations were then used alongside graphical methods to determine the pressures of crystallization for basalt compositions. Kelley and Barton (2008) were able to calculate pressures based on projection of *ol* and *plag* onto the *ol—cpx—qtz* and *plag—cpx—qtz* plane respectively by solving the equations of Yang et al. (1996) simultaneously, and a conversion of liquid compositions into normative mineral

components. These projections were appropriately chosen because the majority of basalt melts are saturated with *ol* and/or *plag*. The pressure of partial crystallization calculated from the method in Kelley and Barton (2008) results from the average of six values, three calculated from *ol*, *plag*, and *qtz* in the *plag* projection and the other three from *plag*, *cpx*, and *qtz* in the *ol* projection. The standard deviation of the six values serves as the uncertainty of this method.

Calculations are performed by a Microsoft Excel program described in Kelley and Barton (2008). The 10 major oxide compositions determined via chemical analysis are used as input data and are automatically fed into the three equations modified from the Yang et al. (1996) mathematical model. Glass analyses are used in preference to whole rock analyses because whole rock analyses could represent mixtures of melt and crystals that could represent xenocrysts or an accumulation of solids in a non-closed system and may generate large pressure errors. Glasses are ideal because they represent quenched melts or the compositions of pre-eruptive liquids in closed systems.

Calculation Error

Accuracy of calculated pressures can be determined by comparing recorded experimental pressures with the calculated pressures of the glasses representing the liquids involved in these experiments. In real world scenarios, error can be introduced by unknown volatile amounts in nominally anhydrous experiments (Kelley and Barton, 2008), but the difference between pressures from these experiments and the calculated pressures can be considered to be the difference between the calculated pressures and the actual pressures of partial crystallization. The accuracy of the method used in this study and detailed in Kelley and Barton (2008) lies within ±126 MPa (1σ). When compared to a method based on one Yang et al. (1996) equation described by (Michael and Cornell, 1998), the Kelley-Barton method used in this study are more accurate as the pressure calculated using the Michael and Cornell (1998) method are accurate to ±160 MPa (1σ) for the same sample set.

Pressure to Depth Conversion

The depth (z) of samples can be derived from the calculated pressures of partial crystallization using the equation:

$$\mathbf{P = \rho * g * z}$$

where **g** represents the acceleration due to gravity and ρ represents the density of the crust. For this study values of 9.8m/s^2 and 2,900 kg/m^3 were used for **g** and ρ respectively. The latter value is an appropriate value for the density of the lower to middle crust beneath the ocean and can be considered as the average density of the oceanic crust beneath Iceland.

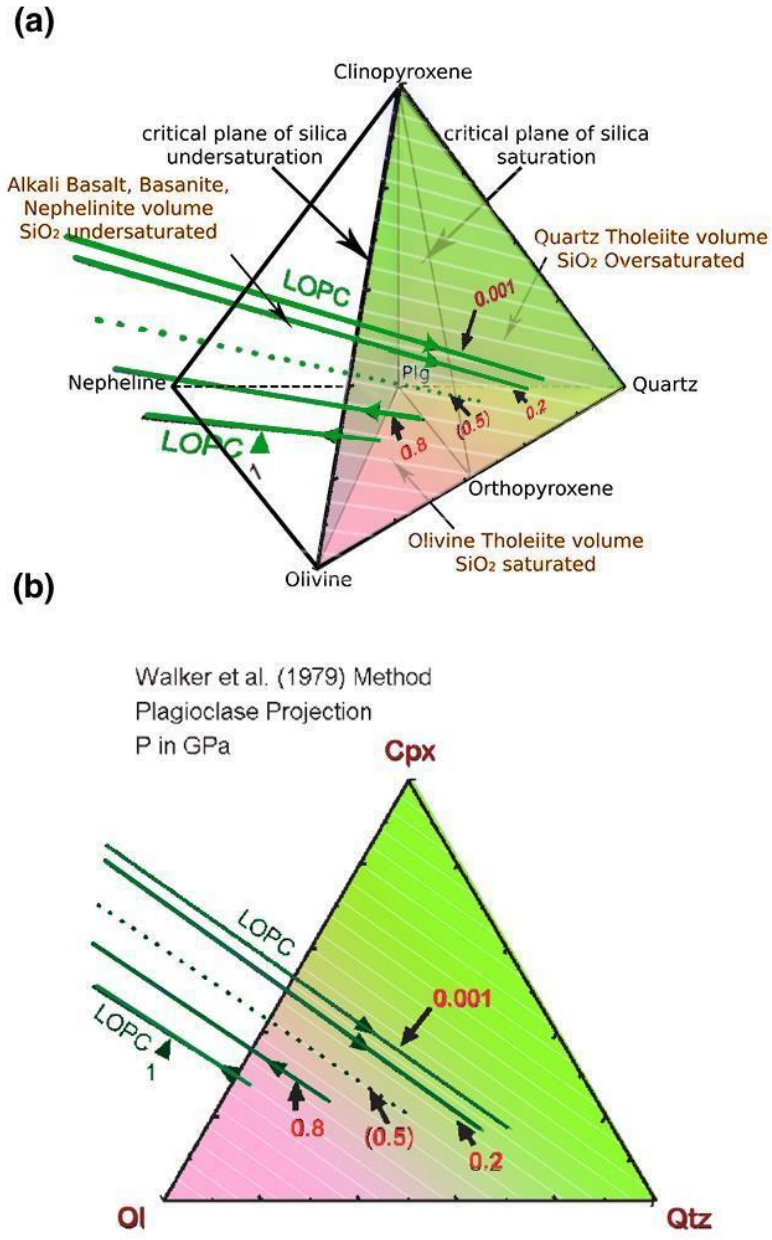

Figure 8: Modified from Kelley and Barton (2008) by Yuyu Li. ***(a)*** *The four major normative minerals: Olivine (ol), Clinopyroxene (cpx), Quartz (qtz), and Nepheline are plotted on a tetrahedron to describe basalt compositions (Yoder and Tilley, 1962). Plagioclase is represented on the nepheline-quartz edge by "Plg". The four-dimensional system used in the Kelley-Barton Method ($CaO—MgO—Al_2O_3—SiO_2$) can be converted to the normative mineral components cpx—ol—plag—qtz. This system is represented by a tetrahedron with cpx, ol, plag, and qtz as the vertices. Phase relationships can be projected from one corner onto the psuedoternary diagrams of the other three minerals.* ***(b)*** *Phase relationships are projected onto the psuedoternary plane ol—cpx—qtz using the Walker et al. (1979) recalculation procedure. The green lines represent the Liquid—Ol—Plg—Cpx—cotectic (LOPC). These lines shift towards ol with increasing pressure on the psuedoternary phase plane ol—cpx—qtz. (*The projection of ol onto plag—cpx—qtz will show a shift in the liquid line of decent towards plag with increasing pressure)*

RESULTS

Partial crystallization pressures were calculated for all glasses from the Kelley and Moore and Calk (1991) datasets. In the absence of filtration, as described in the following section, some samples in these datasets could yield highly erroneous pressures that are unreliable and should not be used for interpretation of the depths of magma chambers. The unfiltered results shown in this section provide the context for the filtering process described in the next section. Descriptions of unfiltered results also reflect the original glass dataset's compositional characteristics.

Figure 9 shows the unfiltered results plotted versus *MgO* content. Relative to other similar studies that have been done different volcanoes, and probably due to the remote nature of the location of Herdubreid, a relatively small number of samples—12 samples from Kelley, but only 9 basalts, and 22 from Moore and Calk (1991) were available for this study. It is therefore difficult to say if these results accurately represent the entirety of the volcanic system under study, but the results can be considered a starting point for interpretations of the data and thus, comparison of these interpretations to the results of studies done using other petrological and non-petrological methods is necessary. Calculated pressures from Moore and Calk (1991) fall in a range of 100 to 700 MPa while calculated pressures from Kelley's dataset fall in a smaller range of 50 to 400 MPa. Grey lines are drawn on each graph in *Figure 9* at pressures of 50 MPa increments to compare the range of values in each dataset. There are no samples in either dataset that produce negative pressures.

There is no single linear correlation between pressure and *MgO* content in the samples involved in this study, as marked by red arrows (*Figure 9*). There are potential inflection points in each dataset at ~8 wt.% although there are no samples with *MgO* content between ~6.8wt.% and ~7.8wt.%. Marked by dashed blue lines, 8 wt.% serves as the inflection point that separates samples of high *MgO* and samples of low *MgO*. In the Moore and Calk (1991) dataset there appears to be a positive correlation for P and *MgO* for high *MgO* samples while in Kelley's dataset there appears to be little or no trend between pressure and *MgO* in samples with high *MgO*. A positive trend (indicating *ol+plag* crystallization) is what we expect for high *MgO* samples. Variation diagrams in *Figure 11* showing the relationships of *CaO* versus *MgO*, Al_2O_3 versus *MgO*, and CaO/Al_2O_3 versus *MgO* also show a turnover around the same value of *MgO*. The variation diagram inflections are interpreted to represent a change in the mineral assemblage of crystallizing liquids. Variations in the data with *MgO* greater than ~8 wt.% represent *ol+plag* crystallization, and variations in data with *MgO* less than ~8 wt.% represent *ol—plag—cpx* crystallization. These trends are consistent with magma evolution via fractional crystallization. The precise *MgO* wt.% inflection points involved in the interpretation part of the Kelley-Barton method have been calculated through regression analyses in other studies though it is not immediately applicable in this study (see the Discussion Section).

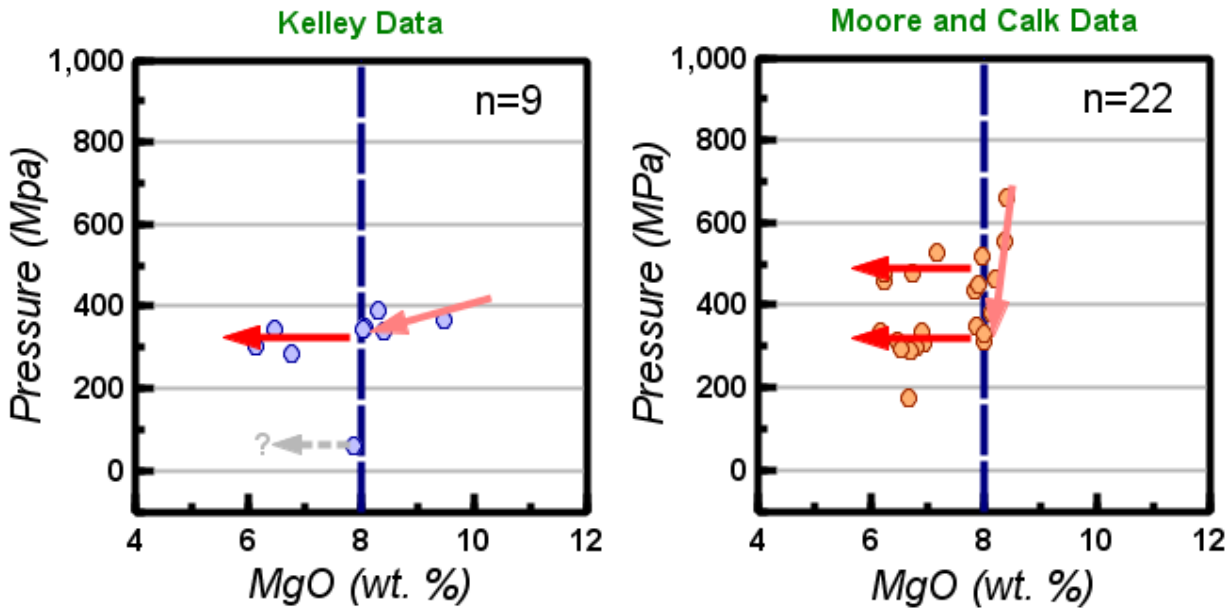

Figure 9: Variation diagrams for the unfiltered datasets of P vs. MgO. Light grey lines mark intervals of 200 MPa. The dark blue dashed lines mark initial interpretations of the turnover point: ~8% MgO where the correlation between Pressure and MgO changes. Two sample groups are marked by arrows: 1) those that crystallize ol±plag (pink arrows) and samples that crystallize ol—plag—cpx (red arrows). A potential cotectic is suggested by the Kelley Data and is marked by the grey dashed arrow.

Discussion

Data Filtration

The Kelley-Barton method was used to calculate pressures of partial crystallization for 31 glass analyses. As mentioned above, the Kelley dataset contained 12 samples but only 9 of them can be classified as basalts. One sample had high Al_2O_3 (30-34%), indicating it is a plagioclase feldspar and 2 others had very high SiO_2 values (72-74%) and are classified as rhyolites. The compositions of these "glasses" are not appropriate for use with the Kelley-Barton method. Therefore, these analyses are filtered out of the data. Methods of filtration are based on the evaluation of errors in the calculation of pressures, consideration of glass compositions, and analysis of chemical variations. The method used in this study is only calibrated for basalt compositions. The filtration process starts with eliminating the results from all non-basaltic samples from the datasets. (Le Bas et al., 1986) defined the composition of basalts and other mafic lavas by plotting Silica (SiO_2) content versus Sodium plus Potassium content (Na_2O + K_2O). The classification parameters used were also used in this study to filter out non-basalts. The visual representation of this step is shown in *Figure 10*.

The next step in the data filtration process is based on the observation that some samples yield unrealistic results in the form of negative pressures. The accuracy of calculated pressures for the Kelley and Barton (2008) method is ±126 MPa. Therefore, pressures of -126 MPa could be calculated from samples that actually crystallized at surface at a pressure of 0.1 MPa and these analyses should not be removed for this reason. Normally, pressures in the range 0 10 -126 MPa would be converted to 0.1 MPa, but in this study none of the samples in either dataset yielded negative pressures within this range. Lack of samples with pressures converted to 0.1 MPa means that there is no concern for data skew for average pressures and interpretations.

The third step in the filtration process is based on the uncertainty of the pressures calculated from each sample. As described in the methods section, the uncertainty (1σ) for the Kelley-Barton method is ±126 MPa. Included in the excel file used to calculate the pressure, the uncertainty was calculated for each sample. Kelley and Barton (2008) states that a pressure associated with a large uncertainty (>±126 MPa) indicates that the glass composition does not correspond to a liquid lying on the *ol—plag—cpx* cotectic, so that such pressures cannot be appropriately included in the interpretation when using this petrologic method. The average values of these errors are described by the general distribution of pressures reported in the "Depth of Magma Chambers" Section.

The final steps of the filtration process are derived from the observation of sample distribution on variation diagrams. Only liquid compositions on the *ol—plag—cpx* cotectic are appropriate for use with the Kelley-Barton method of calculating partial crystallization pressures. Therefore, glass compositions that are representative of liquids in equilibrium with *ol + plag* or *ol* rather than *ol*, *plag*, and *cpx* must be filtered out of the results as they are inconsistent with the Kelley-Barton method. Glass compositions will form a relatively tight, well-defined array on variation diagrams if they lie on the *ol—plg—cpx* liquid line of descent (LLD). Any glass compositions that do not plot within this array can be filtered out of the results as they cannot be confidently considered to lie on the *ol—plag—cpx* LLD. Variation diagrams of CaO, CaO/Al_2O_3, and Al_2O_3, versus vs MgO, are plotted in *Figure 11*. These Oxides, when compared with MgO, best describe compositional differences among *ol*, *plag*, and *cpx*.

Polybaric crystallization, the crystallization of *ol* as melts ascend from the mantle, occurs in nearly all melts (Kelley and Barton, 2008). Polybaric crystallization produces melts that plot directly away from the olivine in a trend that crosses the *ol—plag—cpx* cotectics at various pressures on the pseudoternary plane (*Figure 8b*). Liquids that crystallize *ol—plag—cpx* only exist in a certain pressure range, and therefore no *cpx* crystals form below the upper limit of pressure/depth in this range. *Figure 8b* also illustrates that only *ol ± plag* (and no *cpx*) can crystallize in the area between the *ol—plag—cpx* LLD with the highest pressure and the bottom left apex (*ol*). Therefore, the highest pressure *ol—plag—cpx* is the upper limit along the *ol—plag—cpx* cotectic for pressure of crystallization. In summation, glass compositions not lying on the cotectic cannot be used to accurately calculate pressures of crystallization but can be used as constraints on said pressures.

Diagrams of Pressure (P) vs MgO allow the observation of the change to liquids that crystallize *ol—plag—cpx* from those that crystallize *ol ± plag* but plots of CaO, Al_2O_3, and CaO/Al_2O_3 on separate plots vs MgO are more effective and reliable for examining the same change. The change in trend between low and high MgO samples indicate either evolution via crystallization of *ol ± plag* or by *ol—plag—cpx* crystallization at high P, producing a high *cpx* to *plag* ratio. These trends allow liquids, that crystallize *ol ± plag*, to be distinguished from liquids that crystallize *ol*, *plag*, and *cpx* because the latter liquids show a different positive correlation of CaO, Al_2O_3, and CaO/Al_2O_3 with MgO. The differences in correlations between these two liquids creates a trend with a turnover point between the samples that represent the two different liquids.

After filtration with the three criteria described earlier in this section, the two datasets are plotted in *Figure 11* to determine the inflection point that marks the *ol ± plag* to *ol—plag—cpx* change in crystallization. There are several reasons for the use of the filtered data rather than the non-filtered data for determining the location of the inflection point, the first is that the method only works with basalts and samples representing the compositions of non-basalts are removed in the filtering process. Liquids that produce pressures less than -126 MPa are removed to allow for more accurate comparison between conclusions drawn from variation diagrams and conclusions drawn from plots of Pressure vs MgO. Pressures with 1σ greater than 126 MPa are removed because they can skew the identification of the inflection point and the results from the corresponding samples may be outliers from the trends on Pressure vs MgO diagrams.

A method for finding the inflection point that has been used in a similar study of Hawaiian volcanoes, a senior thesis written by Yuyu Li, is to fit a 2^{nd} order polynomial regression curve to the data in the CaO, Al_2O_3, and CaO/Al_2O_3 vs MgO. However, the relatively small sample size coupled with the scatter in the data causes relatively large uncertainties associated with 2^{nd} order polynomial regression curves and therefore they cannot be considered significant. In this study the inflection point was determined through visual inspection of several variation diagrams in *Figure 11*. There appears to be a weak correlation between high MgO and the other chemical components plotted in *Figure 11* due to scatter but it is possible that this scatter indicates magma evolution along multiple LLDs (Herzberg, 2004; Kelley and Barton, 2008). There are several samples in the Kelley dataset that can be treated as outliers and are not included in the placement of the inflection point determining curves. These inflections not only define the onset of *ol—plag—cpx* cotectic, but also define the LLD for *ol ± plag* crystallization. In this study, this change in crystallization is interpreted to occur at ~8 wt. % MgO as marked on the diagrams in *Figure 11*.

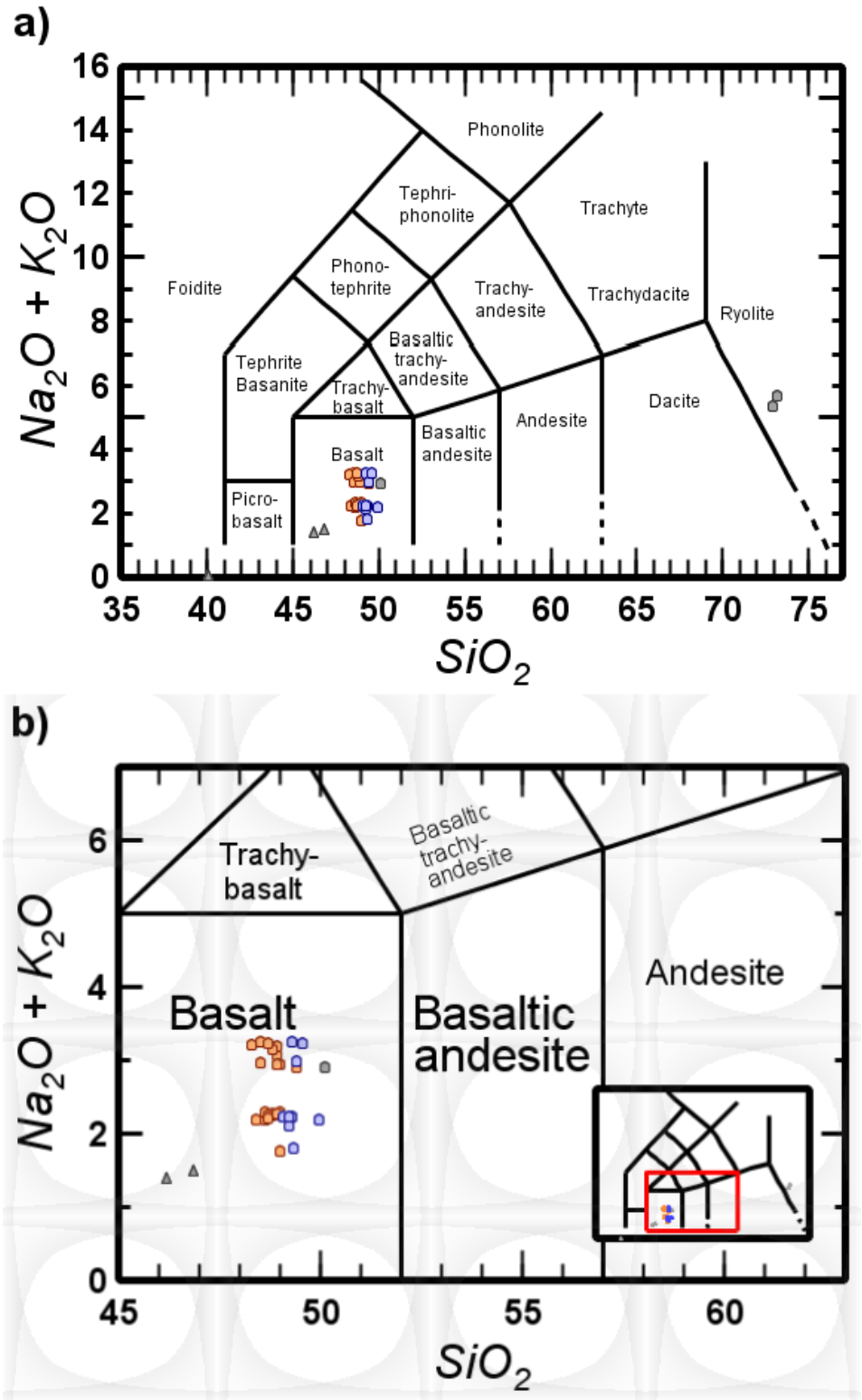

Figure 10: Le Bas et al. (1985) diagrams showing how the compositions of the Kelley (Blue) and Moore and Calk (1991) (Orange) datasets are classified. For comparison, filtered samples are shown as dark grey circles and dark grey circles represent spot analyses that were filtered out. Figure b) is simply an enlarged portion of figure a).

.

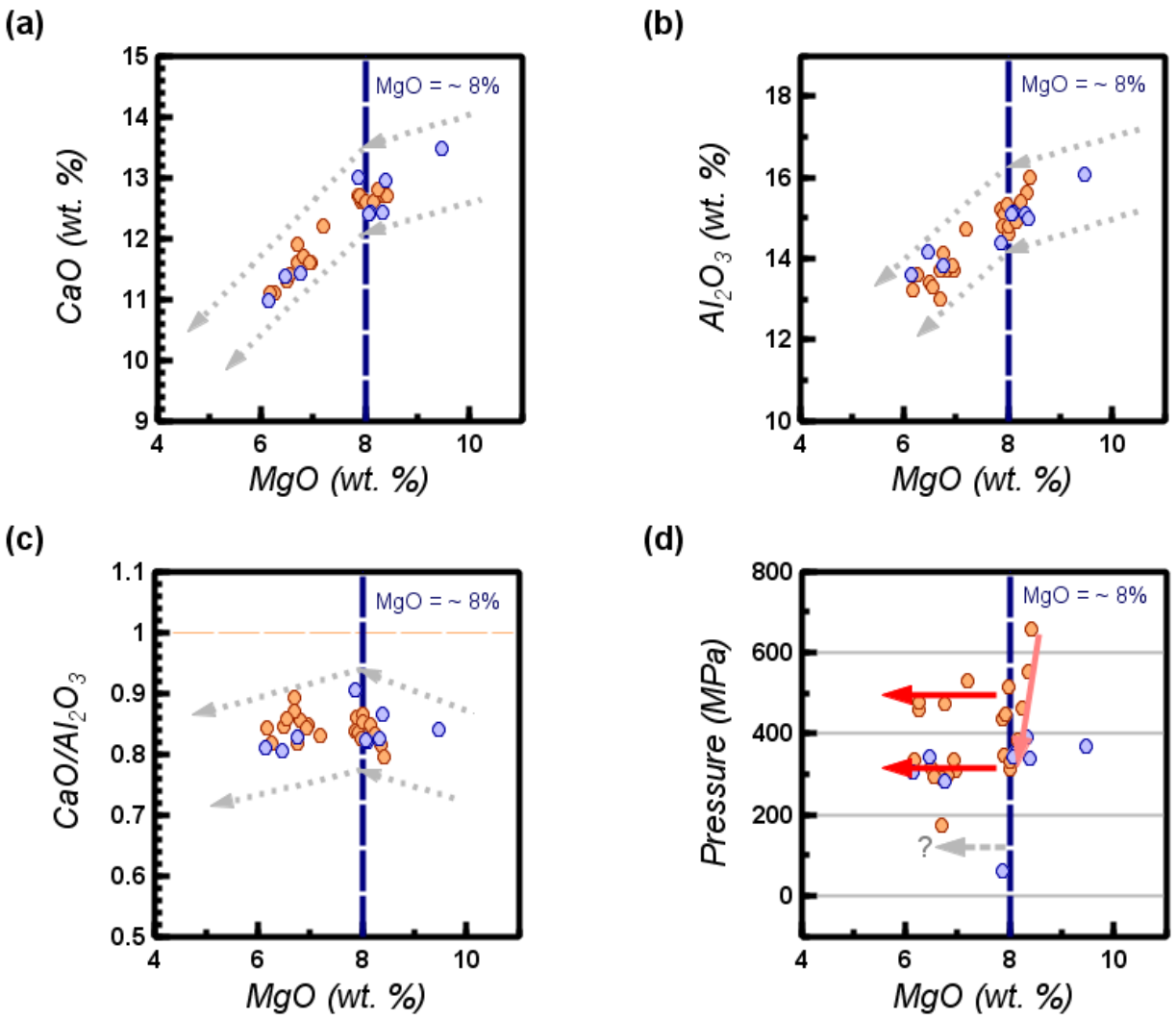

*Figure 11: Variation and diagrams of CaO, Al_2O_3, and CaO/Al_2O_3 vs MgO and P vs MgO for samples that were not removed from the dataset during filtration. The same scale was used for MgO on each of the diagrams for ease of comparison. The Kelley dataset samples are represented by blue circles and the Moore & Calk samples are represented by orange circles. The inflection point of the data is marked on each graph by dark blue dashed lines and marks the difference between Low and High MgO. In **(a)**, **(b)**, and **(c)**, samples lying above these lines in terms of high MgO content crystallize ol—plag and samples with low MgO, lying below these lines, crystallize ol—plag—cpx.*

*In **(a)** and **(b)**, changes in trends of increasing CaO wt. % and Al_2O_3 wt. % with MgO wt. % can be distinguished between the High MgO and Low MgO samples. These trends are marked by dashed grey lines. In **(c)**, the CaO/Al_2O_3 ratio equal to 1 is marked by an orange dashed line. While there are no samples that lie above this line, a CaO/Al_2O_3 ratio > 1 could result from the assimilation of cpx. In **(d)**, red arrows mark a potential trend between Pressure and MgO in high MgO samples and the lack thereof in low MgO samples. A grey dashed arrow continues to mark a potential third cotectic. Without any significant data to back it up however, it cannot be included in the interpretation.*

Interpretation of Calculated Pressures

Insight into magma evolution can be found in the chemical compositions of the glasses. The combination of CaO vs MgO and CaO/Al_2O_3 vs MgO variation diagrams can be used to differentiate among sample compositions in equilibrium with *ol—plag—cpx*, that therefore crystallize along the *ol—plag—cpx* cotectic, and samples in equilibrium with *ol*, that may have crystallized at pressures above the upper bound of *plag* and *cpx* stability. *Figure 11d* shows the relationship between MgO and Pressure for the datasets filtered using the first three conditions. The fourth and final condition involves removing high MgO samples that are interpreted to not carry a signature of *ol*, *plag*, and *cpx* crystallization. In *Figure 11*, these samples lie to the right of the inflection point at ~8% MgO wt. %.

It can be seen that the pressures of partial crystallization for samples that lie on *ol—plag—cpx* cotectics suggest polybaric evolution of magmas beneath Herdubreid. Magma mixing and assimilation complicate the interpretation of calculated pressures and their effects on such calculations are outlined in Kelley and Barton (2008). Magma mixing, between evolved melts and their primitive counterparts lying along the same cotectic, will produce a melt with an intermediate composition that will ultimately not affect the output pressure of partial crystallization. Mixing that occurs between two melts lying along different cotectics, one high pressure and one low pressure, will produce a hybrid melt whose calculated pressure lies in between those of its end-member melts. This type of mixing will therefore reduce the range of calculated pressures that would have otherwise been larger if values for the end member magmas involved in mixing were available. Samples that reflect assimilation of *cpx*-rich gabbroic crust and the simultaneous crystallization of *ol*±*plag* during ascent will yield liquids with higher (typically >1) CaO/Al_2O_3 ratios due to higher CaO concentrations than samples representative of cotectic crystallization alone. As shown by Kelley and Barton (2008), the pressures of partial crystallization calculated from these contaminated melts will be lower than pressures calculated from their uncontaminated counterparts. None of the samples from the filtered database in this study have unusually high CaO contents and all have a CaO/Al_2O_3 ratio <1. Similarly, it has been suggested from the analysis of mid-ocean ridge basalts that dissolution and assimilation of *plag* from gabbroic crust occurs along with ascent-based crystallization of *ol*±*cpx* (Meyer et al., 1985). While these processes will produce magmas with higher Al_2O_3 content and anomalously low CaO/Al_2O_3 ratios (and therefore higher calculated pressures) compared to uncontaminated magmas, none of the samples that passed through the initial filtration produced these anomalous values expected from assimilation and *ol*±*cpx* crystallization.

While there is no apparent evidence for mixing or assimilation from the variation diagrams, magmas in dynamic plumbing systems like those found in Iceland are expected to experience some mixing and interaction with crustal material. It is concluded however, that the results obtained in this study provides no evidence that the wide range of calculated pressures is the result of mixing, assimilation, or a combination of both.

Magma Chamber Depths

The pressures of partial crystallization and their corresponding depths for both datasets used in this study are plotted in *Figure 12* versus MgO wt. %. Samples with MgO content >8% have been included on this plot as Kelley and Barton (2008) suggest that these might be representative of melts that have crystallized in the deep crust or upper mantle. The maximum usable precision

for the Kelley-Barton method is ±126 MPa, but the uncertainty in the pressure for each sample is much lower. The uncertainty in the Kelley sample set is ±26–51 MPa (0.9–1.8 km) with an average of 37 MPa (1.3 km) and the uncertainty in pressure for Moore and Calk (1991) samples is ±40–87 with an average of 67 MPa (2.4 km). Similarly, the accuracy of the Kelley-Barton calculation is ±126 MPa, as discussed in the Methods section, though it is possible that this difference between the actual and apparent pressures could be lower for Icelandic glasses in this study. Further statistical details of the uncertainties by dataset are outlined in *Table 2*.

Partial crystallization depths are calculated from pressures using the equation described in the Pressure to Depth Conversion section of the Methods and assuming constant crustal density at the average density of oceanic crust (2900 kg/m^3). In reality, density of the crust typically increases with depth (Becerril et al., 2013; Mackenzie et al., 1982). With this average density, the upper limit of precision for the method (126 MPa) is 4.43 km. It may be possible to improve the accuracy of depth estimates if better measures of crustal density beneath Herdubreid are available. For this study, the maximum depth calculated at Herdubreid is 18.6 km (527.93 MPa), the minimum depth is 2.1 km (59.16 MPa), and the average is 12.4 km (351.14 MPa). A histogram of sample depths is plotted in *Figure 13* with 1 km bin widths show three depth ranges with high frequency 10–12 km and 15–16 km, suggesting potential magma chambers around those depths.

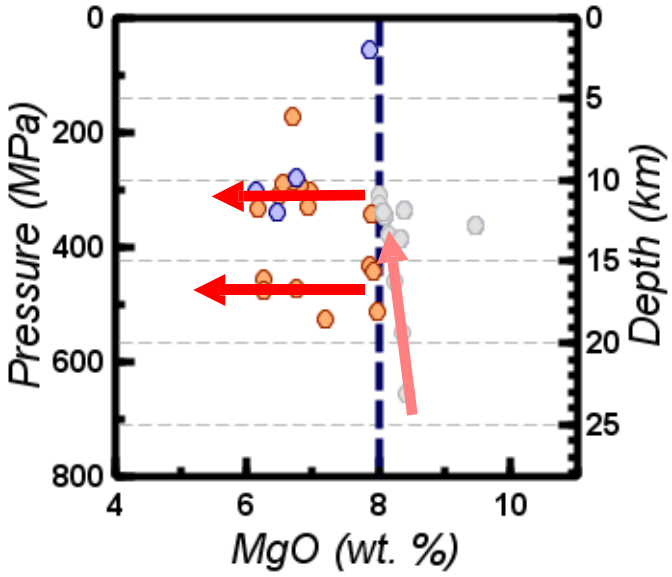

Figure 12: Pressures (P) and depths (z) of filtered results from Dan Kelley and Moore and Calk (1991) datasets plotted vs MgO wt. %. Data determined not to be crystallizing ol—plag—cpx by examination of variation diagram trends is depicted as grey circles. Blue circles represent samples from the Kelley dataset and orange circles represent data from the Moore and Calk (1991) dataset.

Table 2: Summary of Statistics for the Dan Kelley and Moore and Calk (1991) datasets.

Dataset	*Total Number of Samples*	*Number of Samples Filtered Out*	*Pressure Range (MPa)*	*Average Pressure (MPa)*	*Depth Range (km)*	*Average Depth (km)*	*Pressure Uncertainty Range (MPa)*	*Average Pressure Uncertainty (MPa)*	*Depth Uncertainty Range (km)*	*Average Depth Uncertainty (km)*
Dan Kelley	12	3	59.16 – 389.55	307.49	2.1 – 13.7	10.8	26.28 – 50.54	36.53	0.9 – 1.8	1.3
Moore and Calk (1991)	22	5	173.39 – 527.93	375.69	6.1 – 18.6	13.2	40.00 – 87.41	66.98	1.4 – 3.1	2.4
*Combined**	34	8	59.16 – 527.93	351.14	2.1 – 18.6	12.4	26.28 – 87.41	56.02	0.9– 3.1	2.0

**Values calculated for this row were done so using all data in both datasets that were not filtered out.*

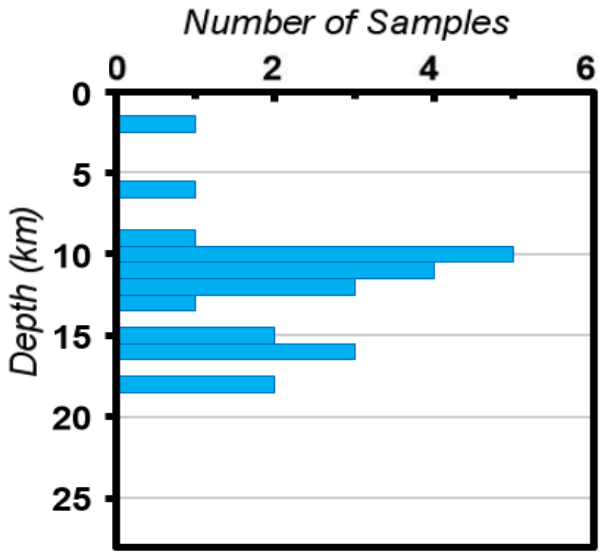

Figure 13: Histogram of calculated depths for both sets of data for Herdubreid with the same scale of depth (down to 28.15 km) as other depth plots. Class width is 1 km. High frequency areas can be seen from 9–11 km and 15–18 km.

Interpretation of Herdubreid's Plumbing System

It is possible to infer the structure of magma plumbing systems from the pressures of partial crystallization calculated from glass analyses, provided the errors associated with these calculations are taken into account. Construction of a consistent model of Herdubreid's (and other Icelandic volcanoes) magma plumbing system(s), requires comparison of the results with those obtained from seismic and GPS geodesy methods. In seismic studies, numbers and depths of magma chambers are estimated through analysis of earthquake swarms, clusters of relatively minor earthquakes, calculated to have occurred at specific depths in the crust. These estimations are based on the assumption that, in volcanic areas, earthquake swarms are the result of magmatic or hydrothermal fluids migrating through previously formed crustal inhomogeneities (Hill, 1977; Toda et al., 2002; Waite and Smith, 2002).

In one study, seismic analysis of earthquake data produced two earthquake clusters at 5 and 15 km depth below Herdubreid and nearby Upptyppingar respectively (Plateaux et al., 2012). The latter of these clusters is suggested to have been the result of deep-seated and rapid magma intrusion while the former is likely due to hydrothermal activity (Jakobsdóttir et al., 2008; Soosalu et al., 2010). Compared to the results of this study, the results in Plateaux et al. (2012) support the presence of a magma reservoir located near 15 km depth beneath Upptyppingar. It is also helpful to compare nearby volcanic systems as these are most likely to have similar subsurface structure to Herdubreid depending on the extent of Herdubreid's local geologic structure. Studies of Herdubreid's structure are limited and opinions vary on whether it is part of the nearby Askja volcanic system or a stand-alone structure formed from the interaction between two systems(Einarsson and Saemundsson, 1987).

A geodetic study of Askja, whose fissure swarm lies near to Herdubreid and may include Herdubreid (See Geologic Setting), found two magma reservoirs beneath the central volcano at 3 and 16 km (Sturkell et al., 2006). It is possible that the upper (3 km) reservoir may be erroneously identified as magmatic in composition in Sturkell et al. (2006), and it is instead analogous to the hydrothermal activity that caused the upper earthquake swarm in Plataeux et al. (2012). However, there is currently no evidence to support that hypothesis and it must be assumed that the original geodetic interpretation is correct when formulating the interpretation in this study. The next logical hypothesis then, is that the upper reservoir beneath Askja is equivalent to the 1–3 km chamber suggested for Herdubreid in this study and a shallower analog for the ~6 km depth chamber suggested by Kelley and Barton (2008). It also follows that the environmental parameters that lead to the formation of Herdubreid's upper reservoir likely also led to that of Askja. A detailed examination of the stratigraphy between the two locations may further prove or disprove this hypothesis but it is not of immediate interest due to the scope of this study.

The second closest volcanic system to Herdubreid is that of Kevrkfjöll, in which a hyaloclastite mountain known as Upptyppingar resides near the northern end ~17 km southeast of Herdubreid and only ~9 km southeast of Herdubreidartögl's southernmost point. A seismic study of Upptyppingar revealed the presence of a magmatic intrusion occurring at 15 km depth (Jakobsdóttir et al., 2008), consistent with the results of this study and other studies done on volcanic systems in the area that are discussed above.

Furthermore, the results of the Kelley and Barton (2008) study agree with the studies listed above. The study determined magma chambers at 6.5 and 18.9 km for Askja which agree with

the geodetic survey of Sturkell et al. (2006). For Herdubreid, reservoirs were interpreted at 10.9 and 17 km depthswith a potential third reservoir at 6.1 km depth (though this was derived from only one sample lying on the cotectic at that position). The maximum depth and the minimum depth in this case agree with the seismic study of Plateaux et al. (2012) and the intermediate chamber is consistent with the data presented in this study.

Therefore, the interpretation of Herdubreid's plumbing system, as shown in the results in this study, is the presence of a magma chamber between 15 and 18 km depth and a shallower magma chamber between 10 and 12 km. The accuracy of this study is validated by comparing and contrasting the results presented here with those of the papers above as visualized in *Figure 14*. There it can be seen that in comparison to *Figure 12* and *Figure 13* the potential reservoir depths interpreted for this study agree with what is expected based on the average interpretations of nearby systems. While it is possible that the crustal structure beneath Herdubreid is locally distinctive and there is no correlation between magma chamber depths of Herdubreid and the systems around it, the lack of evidence for this and the relatively short distance between them make this highly unlikely. This interpretation also provides support for the analysis and interpretation of glass samples from Herdubreid in Kelley and Barton (2008), visualized in *Figure 15* and *Figure 16*. Further examination of the crustal composition may lead to an explanation of the specific depths and provide further insights into the validity of this interpretation, but such an examination lies outside of the scope of this study.

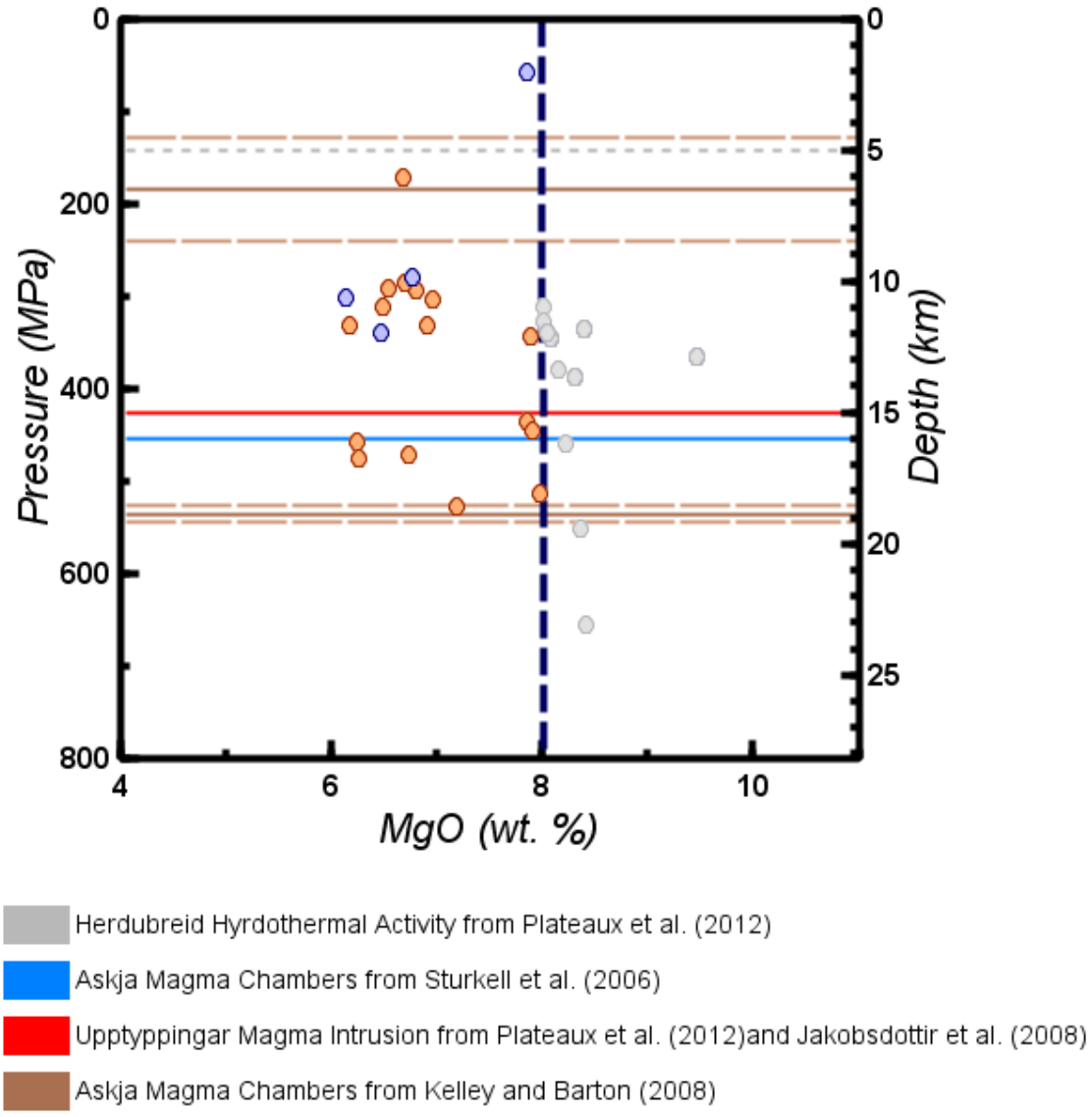

Figure 14: Visual representation of the estimated depths of magma chambers beneath the closest two volcanic systems to Herdubreid, Askja (Kelley and Barton, 2008; Sturkell et al., 2006) and Upptyppingar (Jakobsdóttir et al., 2008; Plateaux et al., 2012), and the proposed hydrothermal activity beneath Herdubreid (presented as a grey dashed line) that caused a fissure swarm similar to one that would occur in a magma chamber (Plateaux et al. 2012). Lighter brown dashed lines around the Kelley and Barton (2008) data indicate the error reported in the interpretation of the magma chambers for Askja.

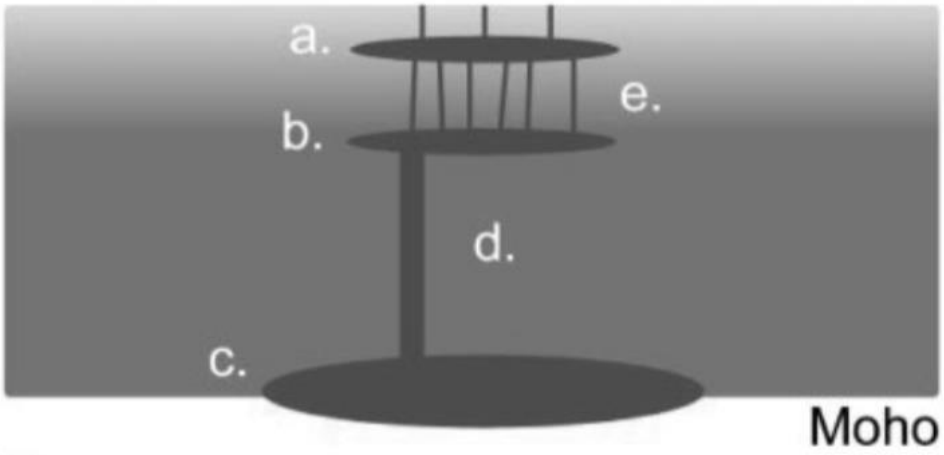

Figure 15: Interpretation of the subsurface structure for Herdubreid taken from Kelley and Barton (2008) in which shallow (a), intermediate (b), and deep chambers (c) are fed by a series of conduits (d) and dikes (e).

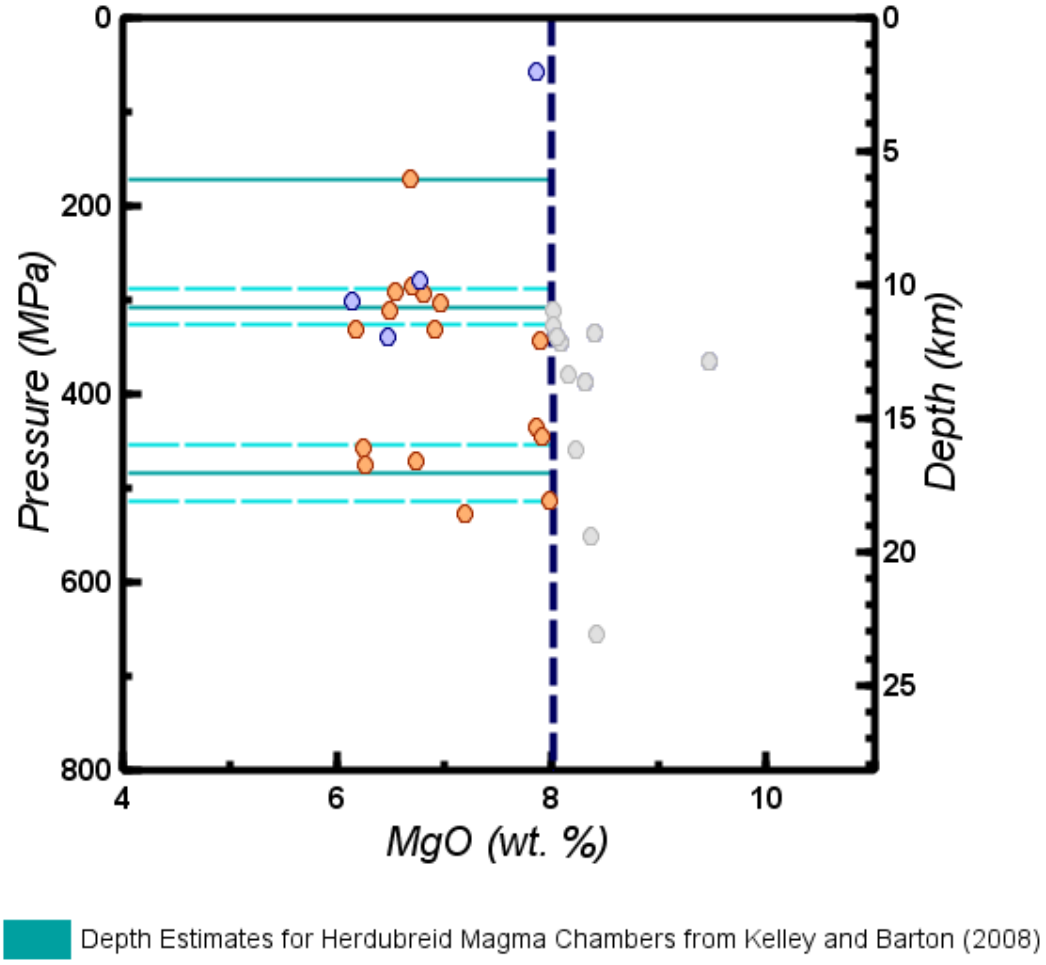

Figure 16: Visualization of the comparison of the interpreted depths of Herdubreid's magma reservoirs and the data used in this study, plotted as MgO vs Pressure and Depth. Lighter blue dashed lines represent the error in the magma chamber depth estimates.

CONCLUSIONS

The pressures of partial crystallization of magmas crystallizing along the *ol—plag—cpx* cotectic, calculated using a petrologic method based on the method described by Kelley and Barton (2008), have been used to estimate the depth of magma chambers beneath the Icelandic volcano Herdubreid. Analyses of basalt glasses, producing major element compositions for the samples, were used as input data as these analyses represent the quenched melts of pre-eruption magma compositions and the calculation method is calibrated for basalts. 126 MPa is the highest acceptable error for this method and serves as the upper limit of accuracy and precision. However, the average error in the data used for this study is only 56.02 MPa and no sample produced a higher error than 87.41 MPa. The CaO, Al_2O_3 and MgO contents are used to distinguish between melts crystallizing *ol—plag—cpx* and those that are crystallizing *ol±plag/cpx*. Models of magma evolution were suggested from examining chemical variations and used to constrain the interpretations of the presence of crustal assimilation, mixing, and polybaric crystallization.

The results of these calculations yielded the interpretation of two magma chambers within the depth ranges of 10–12 km and 15–18 km beneath Herdubreid. This interpretation holds up when compared to chamber depths estimated for nearby volcanic systems using non-petrologic methods that show similar magma reservoir depths in the surrounding central volcanoes and fissure swarms. The original interpretation from Kelley and Barton (2008) agrees with the interpretation presented here, thereby improving confidence in the accuracy and precision of this method when presented with new data.

RECOMMENDATIONS FOR FUTURE WORK

As with most studies containing relatively low amounts of data, it is always useful to continue to analyze and add more samples. More glassy basalt samples and a detailed map of where they were collected would provide insights on current results and those that may emerge from the addition of new data via comparison with known stratigraphy. It would therefore be useful to examine in depth, the stratigraphy of crust beneath Herdubreid and incorporate a more complex model of crustal density, allowing for more accurate calculation of partial crystallization depths. Information on rock units and how they are layered amongst one another could be collected via a combination of seismic testing, field sampling, and gamma ray and resistivity well logs. This stratigraphic information may help us understand why the proposed magma chambers are forming where they are and where we might expect to see magma chambers that are not the result of basaltic magma processes.

The main goal of the overarching project is to get the most complete depiction of Icelandic plumbing systems possible. Therefore, it is necessary to continue compiling data from other volcanic systems, beginning with those closest to Herdubreid for most meaningful comparison, and eventually branching out to include appropriate analogs for the entire Northern Volcanic Zone. This process can then be repeated for each Neovolcanic Zone in Iceland so that they too can be compared and contrasted to observe trends at a macro scale.

Another addition would be to analyze the effect of H_2O. A major assumption for this study was anhydrous conditions. Calculation of pressures for magmas with different water contents would be necessary for examining the degree to which this method is affected by the presence of water. Accounting for H_2O content will allow the calculation of partial crystallization pressure to be more accurate.

REFERENCES CITED

Becerril, L., Galindo, I., Gudmundsson, A., and Morales, J. M., 2013, Depth of origin of magma in eruptions: Scientific Reports, v. 3, p. 6.

Einarsson, P., and Saemundsson, K., 1987, Upptok jardskjalfta 1982-1985 og eldstodvakerfi a Islandi (Earthquake epicenters 1982-1985 and volcanic systems in Iceland): Menningarsjodur.

Gudmundsson, A., 2000, Dynamics of volcanic systems in Iceland: Example of tectonism and volcanism at juxtaposed hot spot and mid-ocean ridge systems: Annual Review of Earth and Planetary Sciences, v. 28, p. 107-140.

Gudmundsson, M. T., Palsson, F., Bjornsson, H., and Hognadottir, p., 2002, The hyaloclastite ridge formed in the subglacial 1996 eruption in Gjalp, Vatnajokull, Iceland: present day shape and future preservation: Geological Society special publication., v. 202, p. 319-336.

Herzberg, C., 2004, Partial crystallization of mid-ocean ridge basalts in the crust and mantle: Journal of Petrology, v. 45, no. 12, p. 2389-2405.

Hill, D. P., 1977, A model for earthquake swarms: Journal of Geophysical Research, v. 82, no. 8, p. 1347-1352.

Hoskuldsson, A., and Sparks, R. S. J., 1997, Thermodynamics and fluid dynamics of effusive subglacial eruptions: Bulletin of Volcanology, v. 59, no. 3, p. 219-230.

Jakobsdóttir, S. S., Roberts, M. J., Guđmundsson, G. B., Geirsson, H., and Slunga, R., 2008, Earthquake swarms at Upptyppingar, north-east Iceland: A sign of magma intrusion?: Studia Geophysica et Geodaetica, v. 52, no. 4, p. 513-528.

Jakobsson, S. P., 1978, Environmental factors controlling the palagonitization of Surtsey tephra, Iceland., Volume 27: Bulletin of the Geological Society of Denmark, Dansk Geologisk Forening (Danish Geological Society), p. 91-105.

Jakobsson, S. P., 1979, Petrology of recent basalts of the Eastern Volcanic Zone, Iceland, Reykjavík, Icelandic Museum of Natural History.

Jones, J. G., 1968, Intraglacial volcanoes of the Laugarvatn region, south-west Iceland--I: Quarterly Journal of the Geological Society Quarterly Journal of the Geological Society, v. 124, no. 1-4, p. 197-211.

Jóhannesson, H., and Sæmundsson, K., 1998a, Geological map of Iceland, 1:500,000. Tectonics.: Icelandic Institute of Natural History and Iceland Geodetic Survey.

Jóhannesson, H., and Sæmundsson, K., 1998b, Geological Map of Iceland, 1:500 000. Bedrock Geology.: Icelandic Institute of Natural History and Iceland Geodetic Survey.

Jóhannesson, H., and Sæmundsson, K., 1999, Geologic Map of Iceland, 1:1,000,000. Bedrock Geology.: National Institute of Natural History and Iceland Geodetic Survey.

Kelley, D. F., and Barton, M., 2008, Pressures of crystallization of Icelandic magmas: Journal of Petrology, v. 49, no. 3, p. 465-492.

Le Bas, M. J., Le Maitre, R. W., Streckeisen, A., and Zanettin, B., 1986, A chemical classification of volcanic rocks based on the total alkali-silica diagram: Journal of Petrology, v. 27, no. 3, p. 745-750.

Mackenzie, K., McClain, J., and Orcutt, J., 1982, Constraints on crustal structure in Eastern Iceland based on extremal inversion of refraction data: Journal of Geophysical Research, v. 87, no. NB8, p. 6371-6382.

Meyer, P. S., Sigurdsson, H., and Schilling, J.-g., 1985, Petrological and geochemical variations along Iceland's Neovolcanic Zones: JGRB Journal of Geophysical Research: Solid Earth, v. 90, no. B12, p. 10043-10072.

Michael, P. J., and Cornell, W. C., 1998, Influence of spreading rate and magma supply on crystallization and assimilation beneath mid-ocean ridges: Evidence from chlorine and major element chemistry of mid-ocean ridge basalts: Journal of Geophysical Research: Solid Earth, v. 103, no. b8, p. 18325-18356.

Moore, J. G., and Calk, L. C., 1991, Degassing and differentiation in subglacial volcanos, Iceland: Journal of Volcanology and Geothermal Research, v. 46, no. 1-2, p. 157-180.

Mortensen, A. K., 2013, Geological Mapping in Volcanic Regions: Iceland as an Example LaGeo: Santa Tecla, El Salvador, p. 12.

Óskarsson, N., Steinþórsson, S., and Sigvaldason, G. E., 1985, Iceland geochemical anomaly - origin, volcanotectonics, chemical fractionation and isotope evolution of the crust: Journal of Geophysical Research-Solid Earth and Planets, v. 90, no. NB12, p. 11-25

Plateaux, R., Bergerat, F., Béthoux, N., Villemin, T., and Gerbault, M., 2012, Implications of fracturing mechanisms and fluid pressure on earthquakes and fault slip data in the east Iceland rift zone: Tectonophysics, v. 581, p. 19-34.

Saunders, A. D., Fitton, J. G., Kerr, J. G., Kerr, A. C., Norry, M. J., and Kent, R. W., 1997, The North Atlantic Igneous Province, *in* Mahoney, J. J., and Coffin, M. F., eds., Large Igneous Provinces: Continental, Oceanic, and Planetary Flood Volcanism: Washington D.C., American Geophysical Union, p. 45-93.

Sigvaldason, G. E., Annertz, K., and Nilsson, M., 1992, Effect of glacier loading deloading on volcanism - postglacial volcanic production-rate of the Dyngjufjöll area, Central Iceland: Bulletin of Volcanology, v. 54, no. 5, p. 385-392.

Soosalu, H., Key, J., White, R. S., Knox, C., Einarsson, P., and Jakobsdottir, S. S., 2010, Lower-crustal earthquakes caused by magma movement beneath Askja volcano on the north Iceland rift: Bulletin of Volcanology, v. 72, no. 1, p. 55-62.

Sturkell, E., Einarsson, P., Sigmundsson, F., Geirsson, H., Ólafsson, H., Pedersen, R., de Zeeuw-van Dalfsen, E., Linde, A. T., Sacks, S. I., and Stefánsson, R., 2006, Volcano geodesy and magma dynamics in Iceland: Journal of Volcanology and Geothermal Research, v. 150, no. 1, p. 14-34.

Thordarson, T., and Höskuldsson, Á., 2002, Iceland, Classic Geology in Europe, Terra Publishing, Harpenden, UK.

Thordarson, T., and Larsen, G., 2007, Volcanism in Iceland in historical time: Volcano types, eruption styles and eruptive history: Journal of Geodynamics, v. 43, no. 1, p. 118-152.

Thórarinsson, S., 1981, Jardeldasvædi á nútíma (Volcanic areas of the Holocene): Náttúra Íslands, Almenna bókafélagid, Reykjavík, p. 81-119.

Tilling, R. I., Heliker, C. C., Wright, T. L., and Geological, S., 1987, Eruptions of Hawaiian volcanoes : past, present, and future, [Reston, Va.?], Dept. of the Interior, U.S. Geological Survey.

Toda, S., Stein, R. S., and Sagiya, T., 2002, Evidence from the AD 2000 Izu islands earthquake swarm that stressing rate governs seismicity: Nature, v. 419, no. 6902, p. 58-61.

Tómasson, H., 1993, Ice-dammed lakes at Kjölur and catastrophic floods in the Hvítá river, southern Iceland (in Icelandic), Volume 62 (1-2): Nát túrufrædingurinn p. 77-98.

Vink, G. E., 1984, A hotspot model for Iceland and the Vöring Plateau: Journal of Geophysical Research, v. 89, no. NB12, p. 9949-9959.

Waite, G. P., and Smith, R. B., 2002, Seismic evidence for fluid migration accompanying subsidence of the Yellowstone caldera: Journal of Geophysical Research-Solid Earth, v. 107, no. B9, p. 17.

Walker, D., Shibata, T., and Delong, S. E., 1979, Abyssal tholeiites from the oceanographer fracture-zone .2. Phase-equilibria and mixing: Contributions to Mineralogy and Petrology, v. 70, no. 2, p. 111-125.

Werner, R., Schmincke, H. U., and Sigvaldason, G., 1996, A new model for the evolution of table mountains: volcanological and petrological evidence from Herdubreid and Herdubreidartögl: Geologische Rundschau, v. 85, no. 2, p. 390-397.

Yang, H. J., Kinzler, R. J., and Grove, T. L., 1996, Experiments and models of anhydrous, basaltic olivine-plagioclase-augite saturated melts from 0.001 to 10 kbar: Contributions to Mineralogy and Petrology, v. 124, no. 1, p. 1-18.

Yoder, H. S., and Tilley, C. E., 1962, Origin of basalt magma - An experimental study of natural and synthetic rock systems: Journal of Petrology, v. 3, no. 3, p. 342-&.

APPENDIX I

Samples from Kelley and Moore and Calk (1991) that were not filtered out.

Dataset	*Date*	*Sample*	*SiO_2*	*Al_2O_3*	*TiO_2*	*FeO*	*MnO*	*MgO*	*CaO*	*Na_2O*	*K_2O*	*P_2O_5*	*Total*	*CaO/Al_2O_3*	*Na+K*	*P (MPa)*	*1σ (MPa)*	*Z (km)*	*1σ (km)*
Kelley	*2015*	*38*	49.27	13.58	2.85	12.96	0.21	6.13	10.97	2.84	0.42	0.27	99.49	0.81	3.26	303.26	48.76	10.7	1.7
Kelley	*2015*	*42b**	49.95	14.39	1.25	10.60	0.19	7.86	13.00	2.07	0.12	0.10	99.54	0.90	2.19	59.16	27.00	2.1	0.9
Kelley	*2015*	*37*	49.41	13.80	2.56	12.40	0.21	6.77	11.40	2.60	0.39	0.24	99.79	0.83	2.99	281.70	51.70	9.9	1.8
Kelley	*2015*	*48(2)*	49.32	16.06	0.71	9.10	0.17	9.47	13.46	1.71	0.08	0.05	100.13	0.84	1.80	365.90	26.28	12.9	0.9
Kelley	*2015*	*36*	49.54	14.15	2.64	12.54	0.23	6.47	11.35	2.79	0.44	0.29	100.43	0.80	3.23	341.29	50.54	12.0	1.8
Kelley	*2015*	*30*	49.28	15.14	1.51	10.49	0.19	8.09	12.41	2.05	0.18	0.13	99.47	0.82	2.23	347.43	27.22	12.2	1.0
Kelley	*2015*	*31**	49.06	15.08	1.50	10.57	0.18	8.32	12.42	2.05	0.19	0.15	99.51	0.82	2.24	389.55	34.19	13.7	1.2
Kelley	*2015*	*32**	49.23	14.99	1.54	10.84	0.17	8.40	12.93	1.95	0.16	0.13	100.34	0.86	2.11	337.43	34.94	11.9	1.2
Kelley	*2015*	*33*	49.21	15.09	1.50	10.48	0.18	8.06	12.39	2.04	0.19	0.15	99.27	0.82	2.23	341.64	28.15	12.0	1.0
M&C	*1991*	*1*	49.00	14.70	2.19	12.50	0.20	7.19	12.20	1.34	0.43	0.33	100.08	0.83	1.77	527.93	54.09	18.6	1.9
M&C	*1991*	*2*	49.00	15.20	1.52	11.10	0.18	7.86	12.70	2.12	0.18	0.23	100.09	0.84	2.30	435.99	51.86	15.3	1.8
M&C	*1991*	*3*	48.80	15.10	1.53	11.10	0.18	7.91	12.60	2.09	0.18	0.22	99.71	0.83	2.27	446.16	49.82	15.7	1.8
M&C	*1991*	*6*	48.60	15.30	1.48	11.10	0.19	7.98	12.60	2.12	0.18	0.22	99.77	0.82	2.30	515.15	54.67	18.1	1.9
M&C	*1991*	*7*	48.50	13.60	2.92	13.40	0.22	6.25	11.10	2.79	0.46	0.36	99.60	0.82	3.25	458.25	81.68	16.1	2.9
M&C	*1991*	*8*	48.30	13.60	2.95	13.40	0.21	6.26	11.10	2.76	0.45	0.36	99.39	0.82	3.21	477.48	80.71	16.8	2.8
M&C	*1991*	*9*	48.50	14.10	2.55	12.60	0.20	6.74	11.50	2.59	0.38	0.35	99.51	0.82	2.97	473.28	70.99	16.7	2.5
M&C	*1991*	*10*	48.90	13.00	2.69	12.70	0.22	6.69	11.60	2.68	0.39	0.27	99.14	0.89	3.07	173.39	87.41	6.1	3.1
M&C	*1991*	*11*	48.90	13.70	2.51	12.40	0.21	6.96	11.60	2.59	0.36	0.25	99.48	0.85	2.95	305.65	67.64	10.8	2.4
M&C	*1991*	*12*	49.00	13.70	2.55	12.50	0.22	6.81	11.70	2.58	0.37	0.28	99.71	0.85	2.95	294.66	67.41	10.4	2.4
M&C	*1991*	*13*	48.90	13.80	2.53	12.40	0.22	6.92	11.60	2.59	0.36	0.27	99.59	0.84	2.95	332.22	66.67	11.7	2.3
M&C	*1991*	*14*	49.40	13.70	2.65	12.90	0.22	6.70	11.90	2.58	0.33	0.28	100.66	0.87	2.91	287.54	64.17	10.1	2.3
M&C	*1991*	*15*	48.90	13.40	2.91	13.10	0.21	6.49	11.30	2.77	0.43	0.27	99.78	0.84	3.20	312.79	75.42	11.0	2.7
M&C	*1991*	*16*	48.80	13.30	2.91	13.00	0.21	6.54	11.40	2.75	0.41	0.29	99.61	0.86	3.16	292.24	79.65	10.3	2.8
M&C	*1991*	*17*	48.70	13.20	2.96	13.40	0.22	6.17	11.10	2.78	0.45	0.32	99.30	0.84	3.23	333.18	79.49	11.7	2.8
M&C	*1991*	*18*	48.80	14.80	1.52	11.10	0.19	7.89	12.70	2.07	0.18	0.16	99.41	0.86	2.25	345.14	40.00	12.1	1.4

*Samples with one spot analyses removed